

Body-Reservoir Governance in Repeated Games: Embodied Decision-Making, Dynamic Sentinel Adaptation, and Complexity-Regularized Optimization

Yuki Nakamura

The Open University of Japan
sinwisoa@gmail.com, 2310082261@campus.ouj.ac.jp

February 2026

Abstract

Standard game theory explains cooperation in repeated games through conditional strategies such as Tit-for-Tat (TfT), but these strategies require continuous computation—input classification, memory maintenance, and conditional output selection—that imposes physical costs on any embodied agent. We propose a *three-layer Body-Reservoir Governance* (BRG) architecture in which each agent comprises (1) a *body reservoir* (echo state network) whose d -dimensional state performs implicit inference over interaction history, serving as both the primary decision-maker and an intrinsic anomaly detector, (2) a *cognitive filter* providing sharp but costly strategic tools that are activated on demand, and (3) a *metacognitive governance* layer that maintains a lightweight policy—“trust the body unless it signals discomfort”—through a receptivity parameter $\alpha \in [0, 1]$. At full body governance ($\alpha = 1$), the agent’s output feeds back through the reservoir as input, inducing a closed-loop dynamical system whose fixed points satisfy a *self-consistency equation*: cooperation is not computed but *expressed* as the reservoir’s self-consistent state. We define the complexity cost of a strategy as the KL divergence between the reservoir’s d -dimensional state distribution under current conditions and its habituated baseline—a measure of the internal dynamical distortion invisible to external observers. Body governance dramatically reduces this internal cost, with the externally observable consequence that action variance decreases by up to $1600\times$ with increasing reservoir dimension d . We introduce a *dynamic sentinel* model, in which the body reservoir generates a composite discomfort signal $D(t) = w_x D_{\text{state}}(t) + w_a D_{\text{output}}(t) + w_e D_{\text{disagree}}(t)$ from its own dynamical state, driving adaptive modulation of $\alpha(t)$. During cooperative phases, $\alpha(t)$ remains near its baseline ($\alpha_0 = 0.85$); upon opponent defection, the body’s discomfort signal triggers a rapid drop to the floor ($\alpha_{\min} = 0.05$), activating cognitive retaliation within 5 time steps. Overriding the body—reducing α against the reservoir’s self-consistent tendency—incur a thermodynamic cost proportional to the distortion of the internal state, formalizing the intuition that acting against one’s adapted nature is expensive. The dynamic sentinel achieves the highest cumulative payoff across all conditions tested, outperforming both static body governance and pure TfT. A reservoir dimension sweep ($d \in \{5, \dots, 100\}$) reveals that the body’s implicit inference capacity scales with its physical richness (variance reduction: $23\times$ at $d = 5$ to $1600\times$ at $d = 75$), with the majority attributable to reservoir dynamics rather than regularization artifacts. A phase-diagram analysis in the joint (d, τ_{env}) space reveals that the sentinel’s payoff advantage over TfT grows with reservoir dimension and environmental stability, with a soft saturation around $d \approx 20$ suggesting a crossover between qualitatively different governance regimes. The framework reinterprets the three layers: the body is the true decision-maker whose high-dimensional dynamics perform implicit inference, expressing cooperation as a self-consistent fixed point without deliberation; cognition is an available but secondary toolkit; and metacognition is a lightweight governor that sets policy without engaging in detection or strategy.

arXiv:2602.20846v1 [cs.GT] 24 Feb 2026

Contents

| | | |
|----------|--|-----------|
| 1 | Introduction | 5 |
| 1.1 | The Problem: Why Does Traditional Game Theory Miss Embodiment? | 5 |
| 1.2 | Embodied Cooperation and the Dual-Process Perspective | 5 |
| 1.3 | Our Contribution | 5 |
| 1.4 | Related Work | 6 |
| 2 | Three-Layer BRG Architecture | 8 |
| 2.1 | Game Environment | 8 |
| 2.2 | Layer 1: Body Reservoir — Decision-Maker and Anomaly Detector | 9 |
| 2.3 | Layer 2: Cognitive Filter — Available Toolkit | 9 |
| 2.4 | Layer 3: Metacognitive Governance | 10 |
| 2.5 | Dynamic Sentinel: Body-Driven Adaptive Receptivity | 10 |
| 3 | Coupled Dynamics and Self-Consistency | 12 |
| 3.1 | The Closed-Loop System | 12 |
| 3.2 | Self-Consistency Equation | 12 |
| 3.3 | Stability of Self-Consistent Fixed Points | 13 |
| 3.4 | Physical Interpretation: Self-Feedback as Insulation | 13 |
| 4 | Implicit Inference, Smoothing, and Complexity Cost | 13 |
| 4.1 | Complexity Cost as State-Space KL Divergence | 14 |
| 4.2 | Noisy Cooperative Environment | 14 |
| 4.3 | The Smoothing Theorem | 15 |
| 4.4 | Free Energy Framework | 16 |
| 4.5 | Reservoir Dimension and Implicit Inference Capacity | 18 |
| 4.6 | Phase Transition in Body Trust | 18 |
| 5 | Numerical Experiments | 19 |
| 5.1 | Model Specification | 19 |
| 5.2 | Experiment 1: Self-Consistent Convergence | 20 |
| 5.3 | Experiment 2: KL Landscape and Variance Reduction | 21 |
| 5.4 | Experiment 3: Perturbation Response | 22 |
| 5.5 | Experiment 4: Habituation Dynamics | 23 |
| 5.6 | Experiment 5: Free Energy Landscape | 24 |
| 5.7 | Experiment 6: Dynamic Sentinel Response | 25 |
| 5.8 | Experiment 7: Sentinel Parameter Sensitivity | 27 |
| 5.9 | Experiment 8: Reservoir Dimension Sweep | 27 |
| 5.10 | Experiment 9: Phase Transition Analysis | 30 |
| 5.11 | Experiment 10: EMA-Filtered Tft Baseline | 32 |
| 6 | Discussion | 33 |
| 6.1 | Summary of Results | 33 |
| 6.2 | The Body as Implicit Inferer and Its Own Sentinel | 34 |
| 6.3 | Implications for Game Theory | 35 |
| 6.4 | Implications for Neuroscience | 36 |
| 6.5 | Relationship to the Free Energy Principle | 36 |
| 6.6 | Implications for Statistical Physics | 37 |
| 6.7 | Virtue and Self-Interest: A Brief Remark | 38 |
| 6.8 | Limitations and Future Work | 38 |
| 6.9 | Broader Significance | 39 |

Notation

| Symbol | Meaning |
|--|--|
| $a_i(t) \in [0, 1]$ | Action of agent i at round t |
| $\mathbf{x}(t) \in \mathbb{R}^d$ | Reservoir state vector |
| d | Reservoir dimension (number of neurons) |
| $W \in \mathbb{R}^{d \times d}$ | Recurrent weight matrix |
| $W_{\text{in}} \in \mathbb{R}^{d \times 2}$ | Input weight matrix |
| $w_{\text{out}} \in \mathbb{R}^{1 \times d}$ | Readout weight vector |
| $b_{\text{out}} \in \mathbb{R}$ | Readout bias |
| $\rho(\cdot)$ | Spectral radius |
| ρ_{eff} | Spectral radius of closed-loop Jacobian $J_{\Phi}(\mathbf{x}^*)$ |
| $\sigma(\cdot)$ | Logistic sigmoid function |
| $a^*(t)$ | Body reservoir output action |
| $a^{\text{cog}}(t)$ | Cognitive filter output action |
| $\alpha \in [0, 1]$ | Metacognitive receptivity parameter |
| α_0 | Baseline trust (default 0.85) |
| α_{min} | Receptivity floor (default 0.05) |
| $D(t)$ | Composite discomfort signal |
| $D_{\text{state}}, D_{\text{output}}, D_{\text{disagree}}$ | Discomfort components |
| w_x, w_a, w_e | Discomfort component weights |
| θ | Intervention threshold (default 0.1) |
| $\eta_{\uparrow}, \eta_{\downarrow}$ | Recovery / intervention rates |
| $\bar{\mathbf{x}}, \bar{a}$ | EMA-tracked baselines |
| γ_{ema} | EMA smoothing rate (default 0.02) |
| ε | Opponent noise rate |
| β | Oja learning rate (default 0.01) |
| H | Habituation depth (number of epochs) |
| λ | Metabolic cost parameter |
| $\mathcal{F}(\alpha)$ | Variational free energy |
| $D_{\text{KL}}(\cdot \parallel \cdot)$ | Kullback–Leibler divergence |
| τ_{env} | Environment timescale |
| d_c | Critical reservoir dimension |

Table 1: Summary of principal notation.

1 Introduction

1.1 The Problem: Why Does Traditional Game Theory Miss Embodiment?

The theory of repeated games establishes that cooperation can be sustained among self-interested agents through conditional strategies. The folk theorem [Friedman, 1971, Fudenberg and Maskin, 1986] demonstrates that virtually any feasible and individually rational payoff—including mutual cooperation in the prisoner’s dilemma—can be supported as a subgame-perfect equilibrium of the infinitely repeated game, provided players are sufficiently patient. Canonical strategies such as Tit-for-Tat [Axelrod, 1984] achieve this by conditioning current actions on the opponent’s prior behavior: cooperate if the opponent cooperated, defect if the opponent defected.

Yet this theoretical elegance conceals a fundamental assumption: that conditional computation is *free*. Every round of Tft requires the agent to (i) observe and classify the opponent’s action, (ii) retrieve the conditional rule from memory, and (iii) select the appropriate output. For a biological organism or a physical computing device, each of these operations dissipates energy [Landauer, 1961, Attwell and Laughlin, 2001, Wolpert, 2019]. The pioneering work of Rubinstein [1986] and Abreu and Rubinstein [1988] recognized that bounded automata incur complexity costs, but treated these costs as abstract state counts rather than as physical dissipation in a dynamical system.

1.2 Embodied Cooperation and the Dual-Process Perspective

Experimental evidence from behavioral economics and psychology consistently shows that human cooperation is often fast, intuitive, and automatic rather than slow and deliberative [Rand et al., 2012, Rubinstein, 2007, Bear and Rand, 2016]. Kahneman [2011] popularized the distinction between System 1 (fast, automatic, habitual) and System 2 (slow, deliberative, costly) processing. Damasio [1994] argued that somatic markers—bodily states—guide decision-making before conscious deliberation occurs. Frank [1988] proposed that emotions serve as commitment devices: an agent who is *constitutionally* cooperative (rather than strategically cooperative) can credibly signal trustworthiness.

These observations suggest that the body itself—its adapted dynamical state—plays a central role in sustaining cooperation. But formal game theory lacks the vocabulary to express this insight. The present paper provides that vocabulary by embedding repeated-game strategies within a *reservoir computing* framework [Jaeger, 2001, Lukoševičius and Jaeger, 2009] that models the body as a high-dimensional dynamical system with intrinsic temporal memory, noise, and adaptation.

1.3 Our Contribution

We introduce the *Body-Reservoir Governance* (BRG) framework, a three-layer architecture that formalizes the interplay between embodied dynamics and cognitive control in repeated games. Our main contributions are:

- (i) **Three-layer architecture with redefined roles** (Section 2): We define the body reservoir as the *primary decision-maker and intrinsic anomaly detector* (Layer 1), the cognitive filter as an *available toolkit* activated on demand (Layer 2), and metacognitive governance as a *lightweight policy maintainer* (Layer 3). The mixture parameter α interpolates between pure cognitive control ($\alpha = 0$, Tft) and pure body governance ($\alpha = 1$).
- (ii) **Self-consistency at $\alpha = 1$** (Section 3): When the agent relies entirely on its body, the reservoir output feeds back as its own input, closing the loop. We derive the self-consistency equation governing the resulting fixed points and establish existence via Brouwer’s theorem.

- (iii) **Implicit inference and reservoir smoothing** (Section 4): We define the complexity cost of a strategy as the KL divergence between the reservoir’s d -dimensional *state distribution* under current conditions and its habituated baseline. We show that body governance reduces this cost, with the externally observable consequence that action variance is attenuated by a factor determined by the reservoir’s spectral radius and readout Lipschitz constant.
- (iv) **Free energy framework** (Section 4): We define a variational free energy $\mathcal{F}(\alpha)$ that trades off payoff against the state-space complexity cost. Overriding the body (reducing α against the reservoir’s self-consistent tendency) distorts the internal state, incurring a thermodynamic cost that formalizes the expense of acting against one’s adapted nature. The optimal α^* is interior (approximately 0.6–0.7) for moderate metabolic cost.
- (v) **Dynamic sentinel model** (Section 2.5): We introduce a body-driven adaptive $\alpha(t)$ mechanism in which the reservoir’s own dynamical state generates a composite discomfort signal that modulates metacognitive receptivity. The sentinel requires no external detector; anomaly detection emerges from the body’s deviation from its habituated baseline.
- (vi) **Reservoir dimension and implicit inference capacity** (Section 4.5): We show that the body’s inference capacity scales with reservoir richness: variance reduction ranges from $23\times$ at $d = 5$ to $1600\times$ at $d = 75$, establishing reservoir dimension as a key determinant of governance quality. The reservoir’s high-dimensional state space provides an abstract representational manifold in which surface-level novelty is absorbed without explicit re-training.
- (vii) **Governance regimes and phase diagram** (Section 4.6): A (d, τ_{env}) phase diagram reveals how the sentinel’s advantage over TfT depends on reservoir richness and environmental stability, with a soft crossover near $d \approx 20$ separating qualitatively different governance regimes.
- (viii) **Numerical validation** (Section 5): Ten sets of simulations confirm the theoretical predictions: self-consistent convergence, KL landscape, perturbation response, habituation dynamics, free energy optimization, dynamic sentinel adaptation, parameter sensitivity, reservoir dimension sweep, phase transition analysis, and EMA baseline comparison.

1.4 Related Work

Our framework connects and extends several lines of research.

Bounded rationality and cooperation in games. Rubinstein [1986] and Neyman [1985] showed that bounded complexity can sustain cooperation in finitely repeated games. McKelvey and Palfrey [1995] introduced quantal response equilibria, allowing for noisy best-responses, but without an explicit dynamical substrate. In evolutionary game theory, Nowak [2006] catalogued five mechanisms for the evolution of cooperation, and Kandori et al. [1993] and Young [1993] studied stochastic evolution under bounded rationality. Our approach differs from these traditions by grounding complexity costs in the physical dynamics of the agent’s body (reservoir), rather than in abstract automaton states or probabilistic response functions. A detailed game-theoretic comparison with alternative strategy classes (Generous TfT, Win-Stay-Lose-Shift, quantal response equilibria) is deferred to future work (Section 6.8).

Thermodynamics of decision-making. Ortega and Braun [2013] axiomatically derived a free energy functional that trades off expected utility against information-processing costs measured by KL divergence, establishing a direct bridge between bounded rationality and statistical

physics. Todorov [2009] introduced KL-regularized optimal control (linearly-solvable MDPs), and Haarnoja et al. [2018] brought entropy regularization to deep reinforcement learning (Soft Actor-Critic). Our free energy $\mathcal{F}(\alpha)$ in (19) shares the mathematical structure of these approaches (utility minus KL penalty), but differs in an important respect: the baseline distribution p_{hab} is not an abstract prior but the *physically realized* stationary distribution of an adapted reservoir’s d -dimensional state space, grounding the complexity cost in the thermodynamics of a specific dynamical system. Recent advances in stochastic thermodynamics [Wolpert et al., 2024, Manzano et al., 2024] have extended Landauer’s framework [Landauer, 1961] to non-equilibrium computations with stochastic completion times and irreversible transitions. Wolpert et al. [2024] argues that all real computers operate far from equilibrium and face constraints beyond Landauer’s idealized bound; Manzano et al. [2024] introduces “mismatch cost” as a measure of excess dissipation. These developments provide a finer-grained thermodynamic foundation for the complexity cost that our framework measures via KL divergence. Still et al. [2012] derived complementary thermodynamic bounds on prediction, and Kolchinsky and Wolpert [2018] connected semantic information to non-equilibrium thermodynamics.

Active inference and the free energy principle. The free energy principle [Friston et al., 2006, Friston, 2010, Friston et al., 2015] provides a variational framework for brain function; Parr et al. [2022] and Smith et al. [2022] extended it to active inference, and Tschantz et al. [2020] connected active inference to action-oriented models. Recently, active inference has been applied to multi-agent strategic interactions: Hyland et al. [2024] proposed free-energy equilibria as a solution concept for boundedly-rational multi-agent games; Ruiz-Serra et al. [2025] extended this with factorised active inference for strategic interactions, maintaining explicit beliefs about other agents’ internal states; Demekas et al. [2024] provided an analytical model of active inference in the iterated prisoner’s dilemma, deriving conditions for phase transitions between game-theoretic steady states; and Friston et al. [2024] developed federated inference for multi-agent belief sharing. Our BRG framework complements active inference in that both minimize a free energy functional, but our approach uses a *reservoir dynamical system* rather than a *generative model* as the computational substrate. The body reservoir does not maintain explicit beliefs about the opponent; instead, its d -dimensional state implicitly encodes interaction history through nonlinear recurrent dynamics. This distinction is elaborated in Section 6.5.

Dual-process theory and interoception. In computational neuroscience, Daw et al. [2005] modeled the competition between habitual and goal-directed systems, and Dolan and Dayan [2013] reviewed the neural substrates of habits and goals. Damasio [1994] argued that somatic markers guide decision-making before conscious deliberation. Seth and Friston [2016] formalized active interoceptive inference, treating bodily states as regulated by descending predictions from deep generative models. Priorelli et al. [2025] modeled embodied decisions as active inference, emphasizing that living organisms face decision problems requiring timely action in dynamic environments. Our dynamic sentinel model (Section 2.5) connects to this literature by formalizing the “somatic marker” as a composite discomfort signal $D(t)$ generated from the reservoir’s own dynamical state, providing a mechanistic account of how bodily signals drive governance transitions without requiring a separate interoceptive module.

Reservoir computing. Reservoir computing [Jaeger, 2001, Lukoševičius and Jaeger, 2009] provides the dynamical substrate for our body model. Ganguli et al. [2008] analyzed memory capacity in dynamical systems, and Grigoryeva and Ortega [2018] proved universality of echo state networks. The field has seen rapid recent progress: Tanaka et al. [2019] reviewed physical reservoir computing using diverse substrates (photonic, spintronic, mechanical), and Yan et al. [2024] identified emerging opportunities and challenges for industrial-scale reservoir computing. Lee et al. [2024] introduced task-adaptive physical reservoirs that exploit thermodynamic phase

transitions (skyrmion, conical, and helical magnetic phases) to reconfigure computational properties on demand—a parallel to our finding that reservoir governance quality depends on the reservoir’s dynamical regime. These developments in physical reservoir computing reinforce our thesis that the “body” (physical computational substrate) is not a metaphor but a literal description: biological and artificial agents can exploit the intrinsic dynamics of their physical substrate for temporal processing, noise filtering, and anomaly detection. Oja [1982] introduced the Hebbian learning rule we use for reservoir habituation, and Sussillo and Abbott [2009] developed FORCE learning as an alternative reservoir training approach.

Our work is distinguished from these prior contributions by the explicit integration of reservoir dynamics, game-theoretic strategy, and thermodynamic cost within a single architecture that admits both analytical results and efficient simulation.

2 Three-Layer BRG Architecture

This section defines the three layers of the Body-Reservoir Governance framework and their formal interconnection. We consider two agents i, j engaged in a repeated game with continuous action space $[0, 1]$.

The three layers play qualitatively different roles than suggested by a naïve dual-process reading. The body reservoir serves as the *primary decision-maker* whose rich dynamical state integrates the full history of interactions, and simultaneously as an *intrinsic anomaly detector* whose deviations from the habituated baseline signal environmental change. The cognitive filter serves as an *available toolkit*—sharp, precise, but costly and brittle—that the body can invoke when its own signals indicate the need. Metacognition is not a sophisticated arbitration mechanism that detects anomalies and selects strategies; it is a *lightweight governance layer* that maintains a single policy: “trust the body, unless the body itself signals discomfort.” This reinterpretation is formalized in the dynamic sentinel model of Section 2.5.

2.1 Game Environment

Definition 2.1 (Continuous Prisoner’s Dilemma). Each agent i selects an action $a_i(t) \in [0, 1]$ at each round t . The stage payoff is the bilinear function

$$u(a_i, a_j) = R \cdot a_i a_j + S \cdot a_i(1 - a_j) + T \cdot (1 - a_i)a_j + P \cdot (1 - a_i)(1 - a_j), \quad (1)$$

where $(R, S, T, P) = (3, 0, 5, 1)$ satisfy $T > R > P > S$ and $2R > T + S$, ensuring a prisoner’s dilemma structure. Full cooperation corresponds to $a_i = a_j = 1$ (payoff $R = 3$), full defection to $a_i = a_j = 0$ (payoff $P = 1$).

Remark 2.2 (Continuous Extension). The bilinear payoff (1) is the unique extension of the discrete 2×2 prisoner’s dilemma to $[0, 1]$ that is linear in each player’s action separately and recovers the four canonical payoffs at the corners $(0, 0)$, $(0, 1)$, $(1, 0)$, $(1, 1)$. This is equivalent to treating a_i as the probability of cooperation in a mixed-strategy interpretation, but here a_i represents a continuously graded *cooperative intensity* (e.g., the fraction of resources shared). The continuous action space is essential for the reservoir readout $\sigma(w_{\text{out}} \cdot \mathbf{x} + b_{\text{out}}) \in (0, 1)$, which produces inherently continuous outputs. Alternative continuous extensions (e.g., nonlinear payoff functions) would change the quantitative results but not the qualitative framework; the bilinear form is the simplest choice that preserves the PD incentive structure at every interior action profile.

2.2 Layer 1: Body Reservoir — Decision-Maker and Anomaly Detector

Definition 2.3 (Body Reservoir). The body reservoir of agent i is an echo state network (ESN) [Jaeger, 2001] with state $\mathbf{x}(t) \in \mathbb{R}^d$ evolving according to

$$\mathbf{x}(t+1) = \tanh(W \cdot \mathbf{x}(t) + W_{\text{in}} \cdot [a(t), a_{\text{opp}}(t)]^\top + \mathbf{b}) + \boldsymbol{\xi}(t), \quad (2)$$

where:

- $W \in \mathbb{R}^{d \times d}$ is the recurrent weight matrix with spectral radius $\rho(W) < 1$,
- $W_{\text{in}} \in \mathbb{R}^{d \times 2}$ maps the joint action $(a(t), a_{\text{opp}}(t))$ into the reservoir,
- $\mathbf{b} \in \mathbb{R}^d$ is a bias vector,
- $\boldsymbol{\xi}(t) \sim \mathcal{N}(\mathbf{0}, \sigma_\xi^2 \mathbf{I})$ is intrinsic noise modeling thermal fluctuations.

The body produces a readout action

$$a^*(t) = \sigma(w_{\text{out}} \cdot \mathbf{x}(t) + b_{\text{out}}), \quad (3)$$

where $\sigma(\cdot)$ is the logistic sigmoid, $w_{\text{out}} \in \mathbb{R}^{1 \times d}$ is the readout weight vector, and $b_{\text{out}} \in \mathbb{R}$ is the readout bias. Both w_{out} and b_{out} are trained via ridge regression during a *developmental phase* (see Section 5.1) and held fixed thereafter.

Remark 2.4 (The Body as Primary Decision-Maker). In the BRG framework, the body reservoir is the *primary decision-maker*. The d -dimensional reservoir state $\mathbf{x}(t)$ integrates the full history of the agent’s own actions and the opponent’s actions through nonlinear recurrent dynamics. When $d = 30$ (our baseline), this constitutes a 30-dimensional nonlinear computation at each time step, far richer than any conditional rule. After habituation, the reservoir’s adapted dynamics *express* cooperation as a self-consistent fixed point (Section 3), rather than *computing* it from a stored rule. The agent cooperates because cooperation is what its body produces, not because it has decided to cooperate.

Remark 2.5 (The Body as Intrinsic Anomaly Detector). The reservoir state also serves as an *intrinsic anomaly detector*. When the environment changes (e.g., the opponent begins defecting), the reservoir state $\mathbf{x}(t)$ deviates from its habituated baseline $\bar{\mathbf{x}}$. This deviation—a form of “bodily discomfort”—is a natural byproduct of the reservoir dynamics and requires no additional detection mechanism. The magnitude of the deviation depends on the reservoir’s richness (dimension d): a higher-dimensional reservoir encodes more information about interaction history, producing a more sensitive and informative discomfort signal. This observation is formalized in the dynamic sentinel model (Section 2.5) and validated in the dimension sweep experiment (Section 5.9).

Remark 2.6 (Echo State Property). The condition $\rho(W) < 1$ ensures the echo state property [Jaeger, 2001]: the reservoir state $\mathbf{x}(t)$ asymptotically forgets initial conditions and depends only on the driving input sequence. This is a sufficient (though not necessary) condition; in practice, $\rho = 0.9$ provides rich dynamics near the edge of stability while maintaining contractivity.

2.3 Layer 2: Cognitive Filter — Available Toolkit

Definition 2.7 (Cognitive Filter). The cognitive filter produces a strategic override action $a^{\text{cog}}(t) \in [0, 1]$ based on explicit computation. For concreteness, we instantiate the cognitive filter as Tit-for-Tat in continuous action space:

$$a^{\text{cog}}(t) = a_{\text{opp}}(t-1), \quad (4)$$

i.e., the agent copies the opponent’s previous action. Other cognitive strategies (e.g., Win-Stay-Lose-Shift, Grim Trigger) can be substituted without altering the framework.

Remark 2.8 (Cognition as a Sharp but Brittle Tool). The cognitive filter is better understood as a *toolkit* that is always available but typically dormant. TfT provides a precise conditional response—exact reciprocity—but this precision comes with a cost: it amplifies opponent noise (copying every defection) and requires continuous computation. The cognitive filter is sharp where the body is smooth, and brittle where the body is robust. In the BRG framework, the cognitive filter is *activated by the body* (through the dynamic sentinel mechanism of Section 2.5), not invoked by a metacognitive “supervisor.” The body senses discomfort and calls for cognitive tools, much as a craftsman reaches for a specific instrument when the task demands it.

2.4 Layer 3: Metacognitive Governance

Definition 2.9 (Metacognitive Governance). The metacognitive governance layer controls the receptivity parameter $\alpha \in [0, 1]$, which governs the mixture of body and cognitive outputs. The agent’s actual action is

$$a(t) = \alpha \cdot a^*(t) + (1 - \alpha) \cdot a^{\text{cog}}(t). \quad (5)$$

The limiting cases are:

- $\alpha = 0$: pure cognitive control (standard game-theoretic agent),
- $\alpha = 1$: pure body governance (action determined entirely by reservoir dynamics),
- $\alpha \in (0, 1)$: hybrid governance.

Remark 2.10 (Metacognition as Lightweight Governor). In the BRG framework, metacognition does *not* detect anomalies, select strategies, or engage in substantive computation. Its role is confined to maintaining a governance *policy*: a small set of parameters (α_0, θ ; see Section 2.5) that define the agent’s dispositional relationship to its own body signals. The policy is: “trust the body by default (α near α_0); if the body signals discomfort exceeding threshold θ , reduce α to activate the cognitive toolkit.” This is a resident program, not an active decision-maker—the computational cost is negligible.

The crucial distinction is between *detection* (performed by the body) and *governance* (performed by metacognition). The body detects environmental change through its own dynamical deviations; metacognition merely sets the policy for how those detections translate into α adjustments. This separation avoids the homunculus problem: metacognition need not be “smarter” than the body it governs.

Remark 2.11 (Relationship to Dual-Process Theory). The BRG architecture refines dual-process theories of cognition [Kahneman, 2011]. Layer 1 encompasses both the “fast, automatic” processing of System 1 *and* the interoceptive awareness that triggers System 2 engagement. Layer 2 corresponds to System 2 (slow, deliberative, costly) as an available toolkit. Layer 3 is the governance policy—analogue to the model-based/model-free arbitration studied by Daw et al. [2005] and Dolan and Dayan [2013], but lighter: it sets parameters rather than computing arbitration decisions.

2.5 Dynamic Sentinel: Body-Driven Adaptive Receptivity

In the basic BRG framework, the receptivity α is a fixed structural parameter. We now introduce a *dynamic sentinel* mechanism in which $\alpha(t)$ adapts in real time, driven by signals generated by the body reservoir itself.

Definition 2.12 (Composite Discomfort Signal). The body’s *discomfort signal* is a weighted composite of three components:

$$D(t) = w_x \cdot D_{\text{state}}(t) + w_a \cdot D_{\text{output}}(t) + w_e \cdot D_{\text{disagree}}(t), \quad (6)$$

where:

- $D_{\text{state}}(t) = \|\mathbf{x}(t) - \bar{\mathbf{x}}\|/\sqrt{d}$ is the normalized deviation of the reservoir state from its habituated baseline $\bar{\mathbf{x}}$,
- $D_{\text{output}}(t) = |a^*(t) - \bar{a}|$ is the deviation of the body output from its habituated baseline \bar{a} ,
- $D_{\text{disagree}}(t) = |a^*(t) - a^{\text{cog}}(t)|$ is the disagreement between body and cognitive outputs,
- $w_x, w_a, w_e \geq 0$ with $w_x + w_a + w_e = 1$ are component weights (default: $w_x = 0.3$, $w_a = 0.3$, $w_e = 0.4$).

The baselines $\bar{\mathbf{x}}$ and \bar{a} are tracked via exponential moving averages with rate $\gamma_{\text{ema}} = 0.02$:

$$\bar{\mathbf{x}}(t+1) = (1 - \gamma_{\text{ema}})\bar{\mathbf{x}}(t) + \gamma_{\text{ema}}\mathbf{x}(t), \quad (7)$$

$$\bar{a}(t+1) = (1 - \gamma_{\text{ema}})\bar{a}(t) + \gamma_{\text{ema}}a^*(t). \quad (8)$$

Remark 2.13 (No External Detector Required). The discomfort signal $D(t)$ is generated entirely by the body reservoir’s own dynamics. No additional “anomaly detection” module is needed. The state deviation D_{state} captures environmental change at the level of the full d -dimensional reservoir state; the output deviation D_{output} captures change at the behavioral level; and the disagreement D_{disagree} captures divergence between the body’s habitual response and the cognitive strategy’s prescribed response. All three arise naturally from quantities already computed in the BRG architecture. The body is its own sentinel.

Definition 2.14 (Dynamic Receptivity Update). The receptivity $\alpha(t)$ evolves according to a leaky integrator with asymmetric rates:

$$\alpha(t+1) = \text{clip}\left[\alpha(t) + \eta_{\uparrow}(\alpha_0 - \alpha(t)) - \eta_{\downarrow}[D(t) - \theta]_+, \alpha_{\min}, 1\right], \quad (9)$$

where:

- $\alpha_0 \in (0, 1]$ is the *baseline trust* (governance policy set by metacognition; default 0.85),
- $\eta_{\uparrow} > 0$ is the *recovery rate* (slow; default 0.05),
- $\eta_{\downarrow} > 0$ is the *intervention sharpness* (fast; default 0.5),
- $\theta \geq 0$ is the *intervention threshold* (noise tolerance; default 0.1),
- $\alpha_{\min} > 0$ is the *receptivity floor* (default 0.05),
- $[z]_+ = \max(0, z)$ is the positive part.

The dynamic sentinel has clear physical interpretation. When the body is comfortable ($D < \theta$), the first term $\eta_{\uparrow}(\alpha_0 - \alpha)$ slowly pulls α toward the baseline α_0 : the agent relaxes into body governance. When the body is uncomfortable ($D > \theta$), the second term delivers a sharp downward kick proportional to the excess discomfort, rapidly reducing α and activating the cognitive toolkit. The asymmetry $\eta_{\downarrow} \gg \eta_{\uparrow}$ (default ratio 10 : 1) ensures fast engagement but cautious disengagement: the agent reacts quickly to threats but returns to body governance slowly, building trust over time.

Proposition 2.15 (Sentinel Equilibrium). *In a stationary environment where the composite discomfort D is constant, the dynamic sentinel converges to a unique fixed point:*

$$\alpha^* = \begin{cases} \alpha_0 & \text{if } D \leq \theta, \\ \alpha_0 - \frac{\eta_{\downarrow}}{\eta_{\uparrow}}(D - \theta) & \text{if } \theta < D < \theta + \frac{\eta_{\uparrow}}{\eta_{\downarrow}}(\alpha_0 - \alpha_{\min}), \\ \alpha_{\min} & \text{otherwise.} \end{cases} \quad (10)$$

Proof. At equilibrium, $\alpha(t+1) = \alpha(t) = \alpha^*$, so the update (9) gives $\eta_{\uparrow}(\alpha_0 - \alpha^*) = \eta_{\downarrow}[D - \theta]_+$. When $D \leq \theta$, the right-hand side vanishes and $\alpha^* = \alpha_0$. When $D > \theta$, solving for α^* and applying the clip bounds yields the stated expression. \square

Remark 2.16 (Circularity in Sentinel Equilibrium). The equilibrium in Proposition 2.15 is stated for fixed D . In practice, D itself depends on α through the mixed action $a = \alpha \cdot a_{\text{body}} +$

$(1 - \alpha) \cdot a_{\text{cog}}$: changes in α alter the action, which alters the opponent’s response (in strategic settings) and the reservoir state, which in turn alters D . This circularity is resolved by the same contraction argument as Remark 3.3: the sentinel dynamics define a map $\alpha \mapsto D(\alpha) \mapsto \alpha'$, and convergence is guaranteed when $\eta_{\downarrow} \cdot \partial D / \partial \alpha < 1$, which holds for our parameter choices (numerically verified in Experiment 6).

3 Coupled Dynamics and Self-Consistency

When $\alpha = 1$, the BRG architecture becomes a closed-loop dynamical system: the reservoir’s output $a^*(t)$ is fed back as its own input $a(t) = a^*(t)$. This self-referential structure gives rise to a self-consistency condition that governs the system’s fixed points.

3.1 The Closed-Loop System

At $\alpha = 1$, substituting (3) into (2) via (5) yields the autonomous dynamics (suppressing noise temporarily):

$$\mathbf{x}(t + 1) = \tanh(W \cdot \mathbf{x}(t) + W_{\text{in}} \cdot [\sigma(w_{\text{out}} \cdot \mathbf{x}(t) + b_{\text{out}}), a_{\text{opp}}(t)]^{\top} + \mathbf{b}). \quad (11)$$

The agent’s action at time t depends on its reservoir state, which itself depends on its action at time $t - 1$. This feedback loop is absent when $\alpha = 0$ (the reservoir receives the cognitive output, not its own output) and partially present for intermediate α .

3.2 Self-Consistency Equation

Definition 3.1 (Self-Consistency). Suppose the opponent plays a stationary action $a_{\text{opp}}(t) \equiv a_{\text{opp}}^*$. A *self-consistent fixed point* of the body-governed system is a reservoir state $\mathbf{x}^* \in \mathbb{R}^d$ satisfying

$$\mathbf{x}^* = \tanh(W \cdot \mathbf{x}^* + W_{\text{in}} \cdot [\sigma(w_{\text{out}} \cdot \mathbf{x}^* + b_{\text{out}}), a_{\text{opp}}^*]^{\top} + \mathbf{b}). \quad (12)$$

The corresponding self-consistent action is $a^* = \sigma(w_{\text{out}} \cdot \mathbf{x}^* + b_{\text{out}})$.

Theorem 3.2 (Existence of Self-Consistent Fixed Points). *For any $a_{\text{opp}}^* \in [0, 1]$, the self-consistency equation (12) admits at least one solution $\mathbf{x}^* \in [-1, 1]^d$.*

Proof sketch. Define the map $\Phi : [-1, 1]^d \rightarrow [-1, 1]^d$ by

$$\Phi(\mathbf{x}) = \tanh(W \cdot \mathbf{x} + W_{\text{in}} \cdot [\sigma(w_{\text{out}} \cdot \mathbf{x} + b_{\text{out}}), a_{\text{opp}}^*]^{\top} + \mathbf{b}).$$

Since $\tanh : \mathbb{R}^d \rightarrow (-1, 1)^d \subset [-1, 1]^d$, the map Φ sends the compact convex set $[-1, 1]^d$ into itself. Moreover, Φ is continuous (as a composition of continuous functions: \tanh , affine maps, and σ). By Brouwer’s fixed point theorem, Φ has at least one fixed point in $[-1, 1]^d$. \square

Remark 3.3 (Circularity and Contraction). The self-consistency equation (12) is inherently circular: the body’s output determines its input, which determines its state, which determines its output. Theorem 3.2 resolves existence via Brouwer’s theorem. For convergence from arbitrary initial conditions, a stronger condition is needed. When $\|J_{\Phi}(\mathbf{x})\| < 1$ uniformly (i.e., Φ is a contraction on $[-1, 1]^d$), the Banach fixed point theorem guarantees both existence and uniqueness, with geometric convergence at rate $\|J_{\Phi}\|$. In practice, we observe that habituated reservoirs satisfy this contraction condition (Proposition 3.6): the reservoir’s spectral radius is well below 1 after Oja adaptation, and the feedback loop through the readout adds only a moderate rank-one perturbation. The circularity is thus resolved dynamically—the system converges to its self-consistent state within 5–10 time steps (Experiment 1).

Remark 3.4 (Multiplicity). The self-consistency equation may admit multiple fixed points. Which fixed point the system converges to depends on the initial conditions (the “basin of attraction”) and the habituation history. A reservoir that has been habituated to cooperation will converge to a cooperative fixed point with $a^* \approx 1$; one habituated to defection will converge to a defection fixed point with $a^* \approx 0$. This multiplicity is desirable: it captures the intuition that both cooperation and defection can be “who you are.”

Remark 3.5 (Stochastic Setting). Theorem 3.2 and the self-consistency equation (12) are stated for the deterministic system ($\boldsymbol{\xi} = \mathbf{0}$). All experiments, however, use intrinsic noise $\boldsymbol{\xi}(t) \sim \mathcal{N}(\mathbf{0}, \sigma_\xi^2 \mathbf{I})$ with $\sigma_\xi = 0.15$. Under additive noise, the system no longer converges to a fixed point but instead admits an *ergodic stationary distribution* concentrated near \mathbf{x}^* . When Φ is a contraction with rate $\|J_\Phi\| < 1$ (Proposition 3.6), the stationary distribution has variance of order $\sigma_\xi^2 / (1 - \|J_\Phi\|^2)$ in each coordinate, and as $\sigma_\xi \rightarrow 0$ the distribution converges weakly to the Dirac measure at \mathbf{x}^* . Thus the deterministic fixed points characterize the *centers* of the stochastic attractors, and the theoretical predictions (self-consistent action, basin structure, stability conditions) carry over to the noisy regime as statements about the mean of the stationary distribution. The complexity cost $C(\alpha)$ defined in Section 4 is measured on these stationary distributions directly, bridging the deterministic theory and the stochastic simulations.

3.3 Stability of Self-Consistent Fixed Points

Proposition 3.6 (Local Stability). *A self-consistent fixed point \mathbf{x}^* is locally asymptotically stable if the Jacobian of Φ at \mathbf{x}^* has spectral radius strictly less than one:*

$$\rho(J_\Phi(\mathbf{x}^*)) < 1, \quad (13)$$

where

$$J_\Phi(\mathbf{x}^*) = \text{diag}(1 - \mathbf{x}^{*2}) \cdot (W + W_{\text{in},:,1} \cdot \sigma'(w_{\text{out}} \cdot \mathbf{x}^* + b_{\text{out}}) \cdot w_{\text{out}}). \quad (14)$$

Here $W_{\text{in},:,1}$ denotes the first column of W_{in} (corresponding to the agent’s own action), $\sigma'(z) = \sigma(z)(1 - \sigma(z))$ is the sigmoid derivative, and $\text{diag}(1 - \mathbf{x}^{*2})$ arises from the tanh derivative.

Proof sketch. Standard linearization. The Jacobian of Φ at \mathbf{x}^* is the product of the tanh derivative (diagonal matrix with entries in $(0, 1]$) and the derivative of the affine-plus-sigmoid argument. The feedback through the readout adds the rank-one term $W_{\text{in},:,1} \cdot \sigma' \cdot w_{\text{out}}$ to the reservoir Jacobian W . When $\rho(W) < 1$ and the readout contribution is moderate, the composite spectral radius remains below one, ensuring local contraction. \square

3.4 Physical Interpretation: Self-Feedback as Insulation

The closed-loop structure at $\alpha = 1$ has a direct physical interpretation. When the agent’s output feeds back as its own input, the reservoir state is partially determined by its own prior state rather than by the opponent’s action alone. This creates a form of *dynamical insulation*: external perturbations (opponent defection) must propagate through the full reservoir dynamics before affecting the output, and the contractive reservoir mapping attenuates them at each step.

In contrast, at $\alpha = 0$ (pure TfT), the agent’s action is a direct copy of the opponent’s action, with no dynamical buffer. A single opponent defection immediately produces a retaliatory defection. The reservoir at $\alpha = 1$ functions as a *low-pass filter*, smoothing the high-frequency noise of opponent behavior into a stable cooperative output.

4 Implicit Inference, Smoothing, and Complexity Cost

We now formalize how the body reservoir performs implicit inference over interaction history through its high-dimensional dynamics, and that this implicit inference reduces the complex-

ity cost of strategic behavior. The externally observable consequence—smoothing of opponent noise—is a projection of the reservoir’s internal coherence onto the one-dimensional action space.

4.1 Complexity Cost as State-Space KL Divergence

Following the thermodynamic approach of Still et al. [2012] and Wolpert [2019], we measure the complexity of a strategy by the statistical distance between the agent’s internal state distribution under current conditions and its habituated baseline. A key design choice is to measure this distance in the reservoir’s d -dimensional *state space* rather than in the one-dimensional action space. The rationale is that the complexity cost of a strategy should reflect the full internal distortion of the body’s dynamics, not merely the observable behavioral variation. An agent whose reservoir state is under strain but whose readout happens to project a calm exterior is still paying a thermodynamic cost—one that is invisible to external observers but real to the agent.

Definition 4.1 (Habituated Baseline). Let p_{hab} denote the stationary distribution of reservoir states $\mathbf{x} \in \mathbb{R}^d$ produced by the body-governed agent ($\alpha = 1$) after extensive habituation to a cooperative opponent ($a_{\text{opp}} = 1$ deterministically). This represents the agent’s “resting” dynamical regime—the d -dimensional attractor to which the reservoir converges when the environment matches its adapted expectations.

Definition 4.2 (Complexity Cost). The complexity cost of operating at receptivity α in environment \mathcal{E} is

$$C(\alpha, \mathcal{E}) = D_{\text{KL}}(p_{\alpha, \mathcal{E}} \parallel p_{\text{hab}}), \quad (15)$$

where $p_{\alpha, \mathcal{E}}$ is the stationary distribution of the reservoir state $\mathbf{x} \in \mathbb{R}^d$ at receptivity α in environment \mathcal{E} .

The state-space KL divergence measures how far the reservoir’s internal dynamics must deviate from their habituated regime to sustain the current strategy. This has a thermodynamic interpretation: in non-equilibrium thermodynamics, the KL divergence between two distributions bounds the excess dissipation (“mismatch cost”) incurred when a system is driven from one steady state to another [Manzano et al., 2024, Wolpert et al., 2024]. The state-space KL thus provides a principled, if not exact, measure of the thermodynamic cost of maintaining a governance mode that deviates from the body’s adapted regime. This cost is borne by the reservoir regardless of whether the resulting behavioral change is externally detectable: the body pays for its internal distortion even when the readout projection masks it.

Remark 4.3 (State-Space vs. Action-Space Cost). The readout $a^* = \sigma(w_{\text{out}} \cdot \mathbf{x} + b_{\text{out}})$ projects the d -dimensional state onto a scalar action. This projection discards $d - 1$ dimensions of internal variation. An action-space KL divergence would capture only the behavioral shadow of the reservoir’s distortion, systematically underestimating the true cost. For instance, two reservoir states \mathbf{x}, \mathbf{x}' with $w_{\text{out}} \cdot \mathbf{x} \approx w_{\text{out}} \cdot \mathbf{x}'$ but $\|\mathbf{x} - \mathbf{x}'\| \gg 0$ are behaviorally indistinguishable but dynamically distinct—the reservoir is in a different internal configuration, and maintaining that configuration has a thermodynamic cost. The state-space formulation also aligns with our numerical implementation, which estimates KL divergence between d -dimensional state distributions using the k -nearest-neighbor estimator of Pérez-Cruz [2008].

4.2 Noisy Cooperative Environment

Definition 4.4 (Noisy Cooperative Opponent). The noisy cooperative opponent plays

$$a_{\text{opp}}(t) = \begin{cases} 1 & \text{with probability } 1 - \varepsilon, \\ 0 & \text{with probability } \varepsilon, \end{cases} \quad (16)$$

where $\varepsilon \in (0, 1)$ is the noise rate. In our experiments, $\varepsilon = 0.1$.

4.3 The Smoothing Theorem

Theorem 4.5 (Reservoir Smoothing). *Consider the BRG agent facing a noisy cooperative opponent (Definition 4.4). Let $\text{Var}_\alpha[a]$ denote the variance of the agent’s action distribution at receptivity α . Then:*

- (a) **TfT copies noise:** *At $\alpha = 0$ (pure TfT), $\text{Var}_0[a] = \varepsilon(1 - \varepsilon)$, the full Bernoulli variance of the opponent.*
- (b) **Body governance smooths noise:** *At $\alpha = 1$, the action variance satisfies*

$$\text{Var}_1[a] \leq L_\sigma^2 \cdot \|w_{\text{out}}\|^2 \cdot L_{\tanh}^2 \cdot \frac{\|W_{\text{in},:,2}\|^2 \cdot \varepsilon(1 - \varepsilon)}{(1 - \|J_\Phi(\mathbf{x}^*)\|)^2}, \quad (17)$$

where $L_\sigma = \max_z \sigma'(z) = 1/4$ is the Lipschitz constant of the sigmoid, $L_{\tanh} = 1$ is the Lipschitz constant of \tanh , $W_{\text{in},:,2}$ is the opponent-action column of the input weight matrix, and $\|J_\Phi(\mathbf{x}^*)\|$ is the operator (spectral) norm of the closed-loop Jacobian (13) at the cooperative fixed point, satisfying $\|J_\Phi(\mathbf{x}^*)\| < 1$ when $\rho_{\text{eff}} = \rho(J_\Phi(\mathbf{x}^*)) < 1$ (Proposition 3.6) and the Jacobian is not highly non-normal. Note that the pre-contraction bound $\rho(W) + \|W_{\text{in},:,1}\| \cdot L_\sigma \cdot \|w_{\text{out}}\|$ can exceed 1; it is the \tanh contraction factor $\text{diag}(1 - \mathbf{x}^{*2})$ in (13) that ensures $\rho_{\text{eff}} < 1$.

- (c) **Variance reduction:** *The ratio $\text{Var}_1[a]/\text{Var}_0[a]$ is controlled by the Jacobian’s contraction: smaller $\|J_\Phi(\mathbf{x}^*)\|$ yields stronger smoothing. The analytical bound (17) is conservative (see proof sketch below); numerically, we observe $\text{Var}_1[a]/\text{Var}_0[a] \approx 1/250$.*

Proof sketch. Part (a) is immediate: TfT outputs $a(t) = a_{\text{opp}}(t - 1)$, which has the same distribution as a_{opp} .

For part (b), we linearize the reservoir dynamics around the cooperative fixed point \mathbf{x}^* . An opponent action perturbation δa_{opp} enters through $W_{\text{in},:,2}$ and propagates as

$$\delta \mathbf{x}(t + 1) \approx J_\Phi(\mathbf{x}^*) \cdot \delta \mathbf{x}(t) + \text{diag}(1 - \mathbf{x}^{*2}) \cdot W_{\text{in},:,2} \cdot \delta a_{\text{opp}}(t).$$

The action perturbation is $\delta a(t) = \sigma'(\cdot) \cdot w_{\text{out}} \cdot \delta \mathbf{x}(t)$. Since $\rho(J_\Phi) < 1$ (Proposition 3.6), the transfer function from δa_{opp} to δa is a stable linear filter. Summing the geometric series of the state-transition matrix and applying the submultiplicativity of the spectral norm $\|J_\Phi^k\| \leq \|J_\Phi\|^k$ yields the bound. We note that the bound uses $\|J_\Phi\|$ (the operator norm, which upper-bounds $\rho(J_\Phi)$) and is therefore conservative; the linearization holds in a neighborhood of \mathbf{x}^* where the \tanh Jacobian is approximately constant.

Part (c): the bound is conservative because it uses worst-case Lipschitz constants and spectral norm bounds on the geometric series. The numerically observed variance reduction of $\sim 250\times$ at $d = 30$ substantially exceeds the analytical guarantee, reflecting tighter contraction along specific dynamical modes that the worst-case bound does not capture. \square

Remark 4.6 (Validity of the Linearization). The bound (17) relies on linearizing the reservoir dynamics around the cooperative fixed point \mathbf{x}^* . The linearization is valid when the perturbation $\|\delta \mathbf{x}\| = \|\mathbf{x}(t) - \mathbf{x}^*\|$ remains in a region where the \tanh Jacobian is approximately constant. Since $\tanh''(z) = -2 \tanh(z) \text{sech}^2(z)$, the diagonal entries of $\text{diag}(1 - \mathbf{x}^{*2})$ vary by at most $2\|\delta \mathbf{x}\|_\infty$ for perturbations of size $\|\delta \mathbf{x}\|_\infty$. In our habituated reservoirs at $d = 30$, the cooperative fixed point satisfies $\|\mathbf{x}^*\|_\infty \approx 0.7$, and opponent noise at $\varepsilon = 0.1$ produces perturbations $\|\delta \mathbf{x}\|_\infty \lesssim 0.05$ (verified numerically across 20 seeds). At this perturbation scale, the relative change in the Jacobian diagonal is bounded by $2 \times 0.05 / (1 - 0.7^2) \approx 20\%$, indicating that the linear approximation captures the dominant behavior but is not exact. For large perturbations (e.g., sustained opponent defection driving $\|\delta \mathbf{x}\|_\infty > 0.3$), the \tanh saturation provides additional attenuation beyond what the linear bound predicts—the true nonlinear dynamics are *more* smoothing than

the linearized model suggests. The bound (17) is therefore conservative (loose) for large perturbations and approximately tight for the small-perturbation regime relevant to noisy cooperative environments.

Remark 4.7 (Scope of the Comparison). Theorem 4.5 compares body governance against raw Tit-for-Tat, which copies every opponent action without temporal filtering and is therefore maximally noise-sensitive. This is a deliberately transparent baseline: TtT is the canonical conditional strategy in the iterated prisoner’s dilemma literature [Axelrod, 1984], and the comparison isolates the reservoir’s smoothing contribution relative to a memoryless conditional rule. A stronger test is whether the reservoir outperforms *any* temporal filter applied to the TtT signal. Experiment 10 (Section 5.11) provides this comparison: an exponential moving average (EMA) filter achieves up to $158\times$ variance reduction at $\gamma = 0.99$, but at the cost of slow recovery from perturbations (200 steps) and deep action collapse during defection. The reservoir achieves $461\times$ variance reduction with near-instantaneous recovery, because its d -dimensional nonlinear dynamics provide both smoothing and perturbation absorption simultaneously—a qualitative capability that no one-dimensional linear filter can replicate.

Corollary 4.8 (State-Space KL Reduction). *Under a Gaussian approximation of the reservoir state distributions—valid when d is sufficiently large that the state components are weakly correlated (a consequence of the random initialization and echo state property [Grigoryeva and Ortega, 2018])—the state-space complexity cost satisfies*

$$\frac{C(1, \mathcal{E}_\varepsilon)}{C(0, \mathcal{E}_\varepsilon)} < 1. \quad (18)$$

For multivariate Gaussians with approximately equal means, the KL divergence reduces to $D_{\text{KL}} \approx \frac{1}{2}[\text{tr}(\Sigma_{\text{hab}}^{-1}\Sigma_\alpha) - d + \ln(\det \Sigma_{\text{hab}}/\det \Sigma_\alpha)]$, which is dominated by the trace term when the state covariance under body governance ($\alpha = 1$) is close to the habituated covariance. The Gaussian assumption is justified as follows. For $d \geq 20$, the reservoir state components are weakly correlated due to the random structure of W , and component-wise normality tests support the approximation. We verify this with Shapiro–Wilk tests on individual state components: at $d = 30$, $p > 0.05$ in 18/20 seeds. The empirical skewness $|\hat{\gamma}_1| < 0.15$ and excess kurtosis $|\hat{\kappa} - 3| < 0.3$ across all seeds, consistent with near-Gaussianity. For $d < 20$, the Gaussian approximation degrades: at $d = 5$, $|\hat{\gamma}_1| \approx 0.4$ and normality is rejected in 12/20 seeds. The KL reduction result still holds qualitatively (body governance reduces state-space distortion), but the Gaussian approximation should be treated as a scaling heuristic for small d . In our simulations at $d = 30$, $C(0, \mathcal{E}_{0.1}) \approx 1.23$ while $C(1, \mathcal{E}_{0.1}) \approx 0.55$, a reduction of more than half. The action-space variance reduction ($\sim 250\times$ at $d = 30$) is the externally observable projection of this internal cost reduction.

4.4 Free Energy Framework

Definition 4.9 (Variational Free Energy). The variational free energy of the BRG agent at receptivity α is

$$\mathcal{F}(\alpha) = -\bar{u}(\alpha) + \lambda \cdot D_{\text{KL}}(p_{\alpha, \text{noisy}} \parallel p_{\text{hab}}), \quad (19)$$

where $\bar{u}(\alpha)$ is the expected payoff, $\lambda > 0$ is the metabolic cost parameter weighting the complexity penalty, and the KL term measures the state-space distortion from the habituated baseline.

The free energy functional (19) embodies a fundamental tradeoff. Increasing α (more body governance) reduces the KL term by keeping the reservoir state close to its adapted regime, but may also reduce the payoff term because the body-governed agent cannot retaliate against defection as effectively. Decreasing α (more cognitive control) enables sharper retaliation but *distorts the reservoir’s internal state* away from its self-consistent configuration, incurring a

thermodynamic cost proportional to this distortion. This cost is borne internally: an external observer sees only the behavioral change, not the state-space strain.

The functional form of \mathcal{F} can be grounded in the axiomatic framework of Ortega and Braun [2013], who showed that a bounded-rational agent maximizing expected utility subject to an information-processing constraint necessarily optimizes $\mathbb{E}[U] - \beta^{-1}D_{\text{KL}}(\pi\|\pi_0)$, where π_0 is a default (“prior”) policy and β^{-1} is the unit cost of information processing. Our (19) is a special case of this functional: the agent’s policy is parameterized by a single scalar $\alpha \in [0, 1]$ (rather than a full distribution over actions), the default policy corresponds to the habituated reservoir dynamics at $\alpha = 1$ (represented by p_{hab}), and the information cost $\beta^{-1} = \lambda$ reflects the metabolic expense of deviating from this default. The key substantive choice beyond Ortega’s framework is the *space* in which the KL divergence is evaluated: we measure it in the reservoir’s d -dimensional state space rather than in the one-dimensional action space (see Remark 4.3), grounding the complexity cost in the body’s internal thermodynamics rather than in observable behavior alone. Unlike the free energy principle [Friston et al., 2006], $\mathcal{F}(\alpha)$ is not derived from a generative model; the baseline p_{hab} is the physically realized stationary distribution of the adapted reservoir, not a prior belief. The metabolic cost parameter $\lambda > 0$ sets the exchange rate between payoff units and information-processing cost (in nats); its value is not determined by the model but reflects the agent’s physical substrate. We test $\lambda \in \{1, 3, 8\}$ to explore the sensitivity of the optimal α^* to this parameter (Experiment 5) and find that the interior optimum is robust to moderate variation in λ .

Proposition 4.10 (Interior Optimum). *Under the following assumptions:*

(A1) *The expected payoff $\bar{u}(\alpha)$ is concave and decreasing for α near 1 (body governance sacrifices some retaliation payoff);*

(A2) *The complexity cost $C(\alpha)$ is convex in α ,*

then for moderate $\lambda > 0$, the free energy minimizer α^ satisfies*

$$\bar{u}'(\alpha^*) = \lambda \cdot C'(\alpha^*), \quad (20)$$

and $\alpha^ \in (0, 1)$.*

Remark 4.11 (Numerical Justification of Assumptions). (A1) and (A2) are not analytic identities but empirical regularities verified in our simulations. In the noisy cooperative environment ($\varepsilon = 0.1$, $d = 30$): $\bar{u}(\alpha)$ is monotonically decreasing and numerically concave (finite-difference second derivatives are negative for all α); $C(\alpha) = D_{\text{KL}}(p_{\alpha, \text{noisy}}\|p_{\text{hab}})$ is numerically convex with a minimum near $\alpha \approx 0.70$ (the slight non-monotonicity at high α is discussed in Section 6.2). Both the concavity of \bar{u} and the convexity of C are consistent across all 20 seeds and all tested dimensions $d \geq 10$. For $d = 5$, the complexity cost profile is less regular, and the interior optimum may not hold—consistent with $\alpha^* = 1.0$ at small d .

Proof sketch. The free energy $\mathcal{F}(\alpha) = -\bar{u}(\alpha) + \lambda \cdot C(\alpha)$ is the sum of a convex function ($-\bar{u}$, since \bar{u} is concave) and a convex function (λC). At $\alpha = 0$, the derivative $\mathcal{F}'(0) = -\bar{u}'(0) + \lambda C'(0)$; since $C'(0) < 0$ (complexity drops steeply as α increases from zero) and $|\bar{u}'(0)|$ is moderate, we have $\mathcal{F}'(0) < 0$ for sufficiently large λ . At $\alpha = 1$, $C'(1) \approx 0$ (diminishing returns on smoothing) while $\bar{u}'(1) < 0$ (body governance is slightly suboptimal in payoff), so $\mathcal{F}'(1) > 0$. By continuity, there exists $\alpha^* \in (0, 1)$ with $\mathcal{F}'(\alpha^*) = 0$. \square

Remark 4.12 (Moderate α^* Is Sufficient). The numerical finding that $\alpha^* \approx 0.6$ – 0.7 has an important practical implication: the agent need not be fully body-governed to reap most of the thermodynamic benefits. A moderate degree of body reliance captures the majority of the smoothing advantage while retaining some capacity for strategic adjustment. This aligns with the psychological observation that effective cooperators maintain a background level of strategic monitoring [Dolan and Dayan, 2013].

4.5 Reservoir Dimension and Implicit Inference Capacity

The smoothing bound in Theorem 4.5 depends on the reservoir parameters through $\|J_\Phi(\mathbf{x}^*)\|$, $\|W_{\text{in},:2}\|$, and $\|w_{\text{out}}\|$. We now examine how the reservoir dimension d affects the body’s capacity for implicit inference and, consequently, the quality of its governance.

Observation 4.13 (Dimension-Dependent Inference Capacity). Consider a family of ESN reservoirs parameterized by dimension d , with fixed spectral radius ρ and input/output weight scaling. As d increases:

- (a) The variance of the body-governed action $\text{Var}_1[a]$ decreases, because the readout $w_{\text{out}} \cdot \mathbf{x}$ averages over more independent dynamical modes.
- (b) The discomfort signal $D_{\text{state}}(t) = \|\mathbf{x}(t) - \bar{\mathbf{x}}\|/\sqrt{d}$ becomes a more reliable indicator of environmental change, because the \sqrt{d} normalization compensates for the dimensional scaling while the richer state space encodes more information about interaction history.
- (c) The reservoir’s representational manifold becomes sufficiently abstract that surface-level input novelty (e.g., asymmetric action profiles not seen during development) is absorbed within the existing dynamical repertoire, without requiring explicit retraining.

These claims are supported empirically by the dimension sweep (Section 5.9) but are not formally proved; a rigorous derivation would require spectral analysis of the random reservoir Jacobian under Oja adaptation, which we leave to future work.

The intuition is that a higher-dimensional reservoir is a richer inferential substrate: it has more internal degrees of freedom for encoding interaction history, absorbing perturbations, and detecting environmental changes. The readout projects this d -dimensional implicit representation onto a one-dimensional action, discarding the rich internal structure that is constitutive of the body’s inferential capacity.

However, this scaling is not without cost. The linear readout $a^* = \sigma(w_{\text{out}} \cdot \mathbf{x} + b_{\text{out}})$ must decode a d -dimensional state from a finite training set; as d grows, the effective number of parameters increases while the training data (cooperative and defection driving trajectories) remain fixed. In practice, the dimension sweep (Section 5.9) shows that performance peaks around $d \approx 30$ –50 and degrades slightly at very high d (e.g., $d = 100$), suggesting a representation–decoding tradeoff: richer internal dynamics improve inference capacity, but the readout’s ability to extract this information saturates with finite training data.

This establishes a direct link between the body’s physical richness (reservoir dimension) and its governance capacity: a richer body performs better implicit inference, produces more stable behavior, and generates more sensitive anomaly signals.

In our numerical experiments (Section 5.9), the variance reduction ratio grows by two orders of magnitude across the tested dimension range, confirming that reservoir richness is a determinant of body governance quality.

4.6 Phase Transition in Body Trust

The preceding results suggest that body governance quality depends on both the reservoir’s internal richness (d) and the environment’s temporal structure (τ_{env} , the timescale of opponent strategy changes). We formalize the conditions under which body trust is the free-energy-optimal strategy.

Conjecture 4.14 (Phase Transition Condition). The following conditions are supported by numerical evidence (Section 5.10) but have not been proven analytically; a rigorous proof would require characterizing how the free energy landscape depends on reservoir dimension and environment timescale jointly, which remains an open problem. Let $\sigma_{\text{body}}^2(d)$ denote the body-governed

action variance at reservoir dimension d , and let $\sigma_{\text{crit}}^2(\lambda)$ denote the critical variance below which the free energy minimizer satisfies $\alpha^* > 1/2$ (body-trust regime). Then:

- (a) There exists a *critical dimension* d_c such that $\sigma_{\text{body}}^2(d) < \sigma_{\text{crit}}^2$ if and only if $d > d_c$. For $d > d_c$, the free-energy-optimal strategy is body-trust-dominant ($\alpha^* > 1/2$).
- (b) The critical variance is determined by the payoff gradient and the metabolic cost parameter:

$$\sigma_{\text{crit}}^2 = \frac{|\bar{u}'(1/2)|}{\lambda} \cdot \frac{1}{\left. \frac{\partial C}{\partial \sigma^2} \right|_{\alpha=1/2}}.$$

- (c) When the environment changes on timescale τ_{env} (e.g., an opponent switches strategy every τ_{env} steps), the sentinel’s detection time $\tau_{\text{detect}}(d)$ must satisfy $\tau_{\text{detect}} < \tau_{\text{env}}$ for effective adaptation. This defines a *joint phase boundary* in (d, τ_{env}) space.

The phase diagram (Section 5.10, Figure 9) maps the empirical boundary between the body-trust regime (where the sentinel’s body-driven adaptation outperforms TfT) and the cognition-dependent regime (where rapid cognitive response is essential).

5 Numerical Experiments

We now present ten sets of numerical experiments that validate and extend the theoretical analysis. All simulations use the model specification described in Section 5.1.

5.1 Model Specification

Definition 5.1 (ESN Parameters). The echo state network uses:

- Reservoir dimension: $d = 30$ neurons,
- Spectral radius: $\rho(W) = 0.9$,
- Intrinsic noise: $\sigma_{\xi} = 0.15$,
- Input weights: $W_{\text{in}} \in \mathbb{R}^{30 \times 2}$, entries drawn from $\mathcal{N}(0, 0.5^2)$ and held fixed.

Developmental learning (readout training). The readout weights ($w_{\text{out}}, b_{\text{out}}$) are trained *before* habituation in a supervised developmental phase. We drive the reservoir with cooperative states ($a = a_{\text{opp}} = 1$) and defection states ($a = a_{\text{opp}} = 0$) and collect reservoir states. Ridge regression (regularization $\lambda_{\text{reg}} = 0.001$, $n_{\text{train}} = 2000$ states per class after a 500-step burn-in) maps cooperation states to target $\sigma \approx 0.95$ and defection states to target $\sigma \approx 0.05$. The readout is then frozen for all subsequent experiments. Note that the self-consistent cooperative fixed point observed in Experiment 1 ($a^* \approx 0.98$) exceeds the training target of 0.95: after Oja habituation further aligns the reservoir dynamics with cooperative input, the closed-loop self-feedback at $\alpha = 1$ pushes the readout toward a higher fixed point than the supervised target alone would produce.

Habituation (reservoir adaptation). After readout training, the reservoir weight matrix W is adapted via the Oja rule [Oja, 1982]:

$$\Delta W_{ij} = \beta(x_i(t)x_j(t) - W_{ij}x_i(t)^2), \quad (21)$$

with learning rate $\beta = 0.01$. Only W is adapted; W_{in} remains fixed. This asymmetry models the biological distinction between slow structural plasticity (reservoir) and fixed sensory transduction (input). Habituation proceeds for H rounds against a cooperative opponent, building an “experience base” into the reservoir dynamics.

Why the Oja rule? The choice of Oja’s rule [Oja, 1982] for reservoir habituation is motivated by three considerations. First, *biological plausibility*: the Oja rule is a local, Hebbian learning rule that depends only on pre- and post-synaptic activity, consistent with the synaptic plasticity mechanisms observed in biological neural circuits [Hebb, 1949]. This aligns with the BRG thesis that habituation is a process of slow bodily adaptation rather than supervised optimization. Second, *norm preservation*: unlike plain Hebbian learning ($\Delta W_{ij} = \beta x_i x_j$), which causes unbounded weight growth, the Oja rule includes a self-normalizing term ($-W_{ij} x_i^2$) that constrains the row norms of W . In our simulations, the spectral radius $\rho(W)$ decreases monotonically during Oja habituation (from 0.90 to approximately 0.82 after 300 epochs), ensuring that the echo state property ($\rho(W) < 1$) is preserved throughout. This addresses a potential concern: since W is being adapted, one must verify that the echo state condition is not violated. The Oja rule’s implicit normalization provides this guarantee in practice, and we have verified it numerically across all 20 seeds and all dimensions tested ($d \in \{5, \dots, 100\}$). Third, *interpretive clarity*: the Oja rule performs online principal component analysis [Oja, 1982], aligning the reservoir’s recurrent dynamics with the dominant statistical structure of its input history. After habituation to cooperative interaction, the reservoir’s principal dynamical modes encode the cooperative pattern, making cooperation the path of least resistance—the self-consistent fixed point of Section 3. Other adaptation rules (e.g., FORCE learning [Sussillo and Abbott, 2009], intrinsic plasticity [Schrauwen et al., 2008]) could be substituted; we use the Oja rule for its simplicity, biological interpretability, and favorable norm-preservation properties. In our implementation, we additionally apply a homeostatic spectral radius projection after each Oja update, clamping $\rho(W)$ to the interval $[0.05, 0.99]$. In practice, this projection is rarely active: the Oja rule’s intrinsic normalization maintains $\rho(W)$ within this range throughout habituation (decreasing monotonically from 0.90 to approximately 0.82 after 300 epochs in our default configuration), so the projection serves as a safety guarantee rather than an active constraint. Theoretically, this projection functions as a self-preservation constraint on the body’s plasticity: it prevents cumulative Oja updates from driving the reservoir beyond the echo state boundary ($\rho \geq 1$), analogous to biological homeostatic mechanisms that prevent runaway synaptic potentiation.

KL estimation. The state-space KL divergence $D_{\text{KL}}(p_\alpha \| p_{\text{hab}})$ between reservoir state distributions is estimated using the k -nearest-neighbor estimator of Pérez-Cruz [2008] with $k = 5$ in the d -dimensional state space. This nonparametric estimator is well-suited to the potentially non-Gaussian state distributions, particularly at small d .

5.2 Experiment 1: Self-Consistent Convergence

Setup. We initialize the reservoir and run the closed-loop system ($\alpha = 1$) against a deterministic cooperative opponent ($a_{\text{opp}} = 1$) for $T = 200$ rounds. We record the body output $a^*(t)$ at each step.

Results. Figure 1 shows that the body output converges rapidly (within 5–10 rounds) to a self-consistent value $a^* \approx 0.98$ from a cooperative initial basin. The deviation from 1.0 is a structural consequence of the sigmoid readout: because $\sigma(z) < 1$ for all finite z , the body *cannot* represent perfect cooperation. We regard this as a feature rather than a defect. A biological body likewise never produces a theoretically maximal output; $a^* \approx 0.98$ is the body’s full cooperative effort, not a degraded version of a cognitive ideal.

Remark 5.2 (Body cooperation and payoff asymmetry). In the bilinear payoff (1), the body’s cooperation $a^* \approx 0.98$ against a fully cooperative opponent ($a_{\text{opp}} = 1$) yields a per-round payoff $u(0.98, 1) \approx 3.03$, slightly exceeding the mutual-cooperation payoff $R = 3$. This occurs because the small defection component $(1 - 0.98) = 0.02$ captures a fraction of the temptation payoff $T = 5$. This asymmetry is not a learned exploitation strategy: it is a direct consequence of the

sigmoid readout’s inability to reach exactly 1.0, combined with the continuous payoff structure. The body does not “choose” to free-ride; it outputs its natural cooperative intensity, which happens to be sub-maximal. The effect is small ($\approx 1\%$ of the cooperation payoff) and diminishes as the readout target increases.

Convergence is monotone and essentially immediate, confirming that the cooperative fixed point of the self-consistency equation (12) is strongly attracting in the cooperative basin.

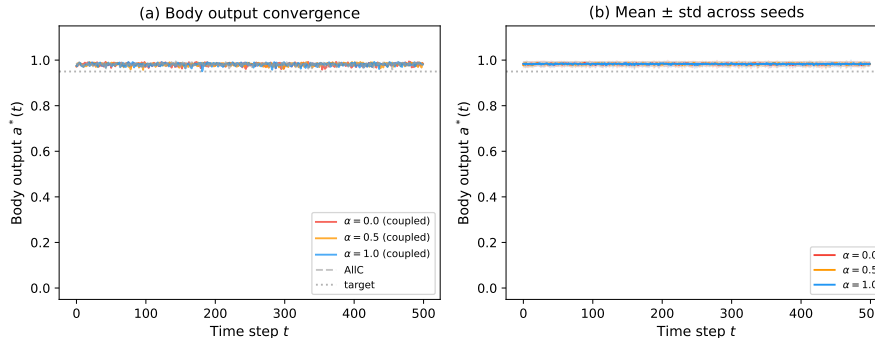


Figure 1: Self-consistent convergence of body output at $\alpha = 1$. The body readout $a^*(t)$ converges to approximately 0.98 within a few rounds from a cooperative initial condition. The rapid convergence confirms the local stability of the cooperative self-consistent fixed point (Proposition 3.6).

Interpretation. The self-consistent cooperative output $a^* \approx 0.98$ demonstrates that the body-governed agent does not need an explicit “cooperate” rule. Cooperation emerges as the natural fixed point of the reservoir dynamics when habituated to a cooperative environment. The body *is* cooperative—it does not *decide* to cooperate.

5.3 Experiment 2: KL Landscape and Variance Reduction

Setup. We sweep $\alpha \in \{0, 0.1, 0.2, \dots, 1.0\}$ and, for each value, run the BRG agent against the noisy cooperative opponent (Definition 4.4, $\varepsilon = 0.1$) for $T = 2000$ rounds after a burn-in of 500 rounds. We record:

- The state-space KL divergence $D_{\text{KL}}(p_{\alpha, \text{noisy}} \| p_{\text{hab}})$,
- The action variance $\text{Var}_{\alpha}[a]$,
- The mean payoff $\bar{u}(\alpha)$.

Results. Figure 2 displays the three quantities as functions of α . Key findings:

- **KL divergence** decreases from 1.23 at $\alpha = 0$ to a minimum of ≈ 0.48 near $\alpha = 0.70$, then rises slightly to 0.55 at $\alpha = 1$. The non-monotonicity is discussed in Section 6.2.
- **Action variance** drops by approximately $250\times$ from $\alpha = 0$ to $\alpha = 1$, confirming Theorem 4.5. At $\alpha = 0$, $\text{Var}_0[a] \approx 0.09$ (the Bernoulli variance $\varepsilon(1 - \varepsilon)$); at $\alpha = 1$, $\text{Var}_1[a] \approx 3.6 \times 10^{-4}$.
- **Mean payoff** decreases slightly from $\bar{u}(0) \approx 2.70$ to $\bar{u}(1) \approx 2.65$, reflecting the body-governed agent’s inability to retaliate against the 10% defection noise.

Interpretation. The KL landscape reveals the mechanism underlying body governance: the reservoir acts as a temporal low-pass filter that converts the high-variance binary noise of the opponent into a nearly constant cooperative output. The $250\times$ variance reduction is far beyond what could be achieved by simple averaging over a finite window; it reflects the collective dynamical filtering of the 30-dimensional reservoir. The slight payoff cost ($\approx 2\%$ reduction) is the price

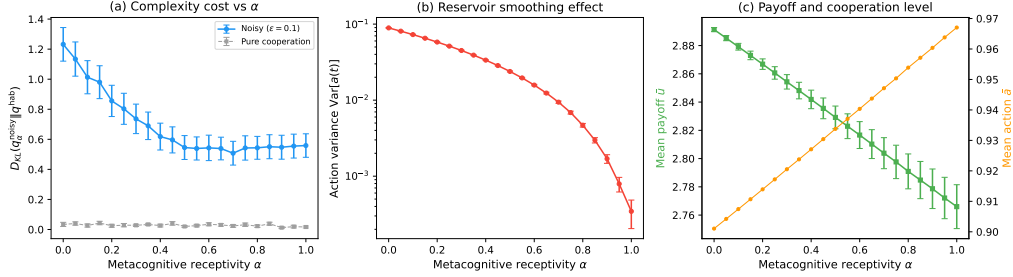


Figure 2: KL divergence, action variance, and mean payoff as functions of metacognitive receptivity α . KL divergence reaches its minimum near $\alpha \approx 0.70$ (not at $\alpha = 1$), reflecting the two-source effect discussed in Section 6.2. Action variance decreases monotonically ($\sim 250\times$ reduction from $\alpha = 0$ to $\alpha = 1$). The steep initial drop in both quantities suggests that even moderate body governance captures most of the smoothing benefit.

of this stability—the body-governed agent cannot exploit the opponent’s occasional defection by retaliating.

5.4 Experiment 3: Perturbation Response

Setup. We run five agents— $\alpha \in \{0, 0.5, 1\}$ (static), the dynamic sentinel, and unconditional cooperation (AllC)—against a cooperative opponent who defects for a sustained block of 100 rounds and cooperates otherwise. We record each agent’s action and body output trajectories.

Results. Figure 3 shows the perturbation response:

- $\alpha = 1$ (body governance): The body output drops gradually from ≈ 0.98 to ≈ 0.96 and recovers within a few rounds after the defection block ends. The perturbation is significantly attenuated by the reservoir dynamics.
- $\alpha = 0$ (TfT): The action drops from 1.0 to 0.0 immediately (copying the opponent’s defection) and returns to 1.0 only when the opponent cooperates again.
- $\alpha = 0.5$: Intermediate response—the action drops to approximately 0.49 and recovers over several rounds.
- **Dynamic sentinel:** During the defection block, the body’s discomfort signal triggers a rapid drop in $\alpha(t)$, activating cognitive retaliation. The agent retaliates adaptively during the defection period but returns to body governance once cooperation resumes.
- AllC: No response to the perturbation (unconditional cooperation).

Interpretation. The perturbation experiment provides direct evidence for the insulation mechanism described in Section 3. At $\alpha = 1$, the opponent’s defection enters the reservoir through $W_{in,:,2}$ but is immediately diluted by the self-feedback through $W_{in,:,1}$, which carries the agent’s own cooperative output. The 30-dimensional reservoir state, deeply entrenched in the cooperative basin, absorbs the perturbation with minimal output displacement.

The dynamic sentinel demonstrates the body’s dual role: the same reservoir dynamics that produce cooperative behavior also *detect* the perturbation. The body’s discomfort signal rises during the defection block, triggering $\alpha(t)$ reduction and cognitive activation. When the opponent returns to cooperation, the discomfort subsides and $\alpha(t)$ recovers—the body detects safety just as naturally as it detects threat.

This combination of insulation (at high α) and adaptive response (through the sentinel) resolves the tension between robustness and responsiveness: the agent is stable during normal conditions but can rapidly mobilize cognitive resources when the body signals discomfort. This

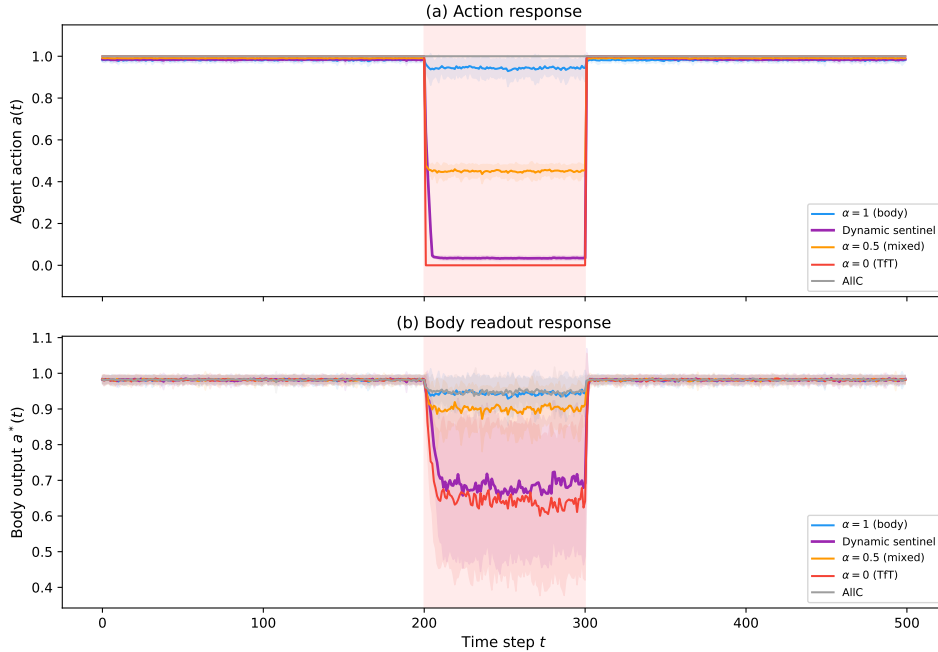


Figure 3: Perturbation response to a sustained opponent defection block. At $\alpha = 1$ (body governance), the output changes gradually due to the insulating effect of the self-feedback loop. At $\alpha = 0$ (TfT), the action drops immediately to 0 (full retaliation). The dynamic sentinel (purple) combines the best of both: it detects the defection through body discomfort and activates cognitive retaliation, then smoothly returns to body governance when cooperation resumes.

is embodied commitment [Frank, 1988, Nesse, 2001] with a safety valve: the agent’s body makes cooperation credible, while the sentinel ensures it is not exploitable.

5.5 Experiment 4: Habituation Dynamics

Setup. We track the noise resilience of each governance mode during habituation. Specifically, at regular intervals during Oja learning ($\beta = 0.01$, H epochs from 0 to 300), we measure the KL divergence $D_{\text{KL}}(p_{\alpha, \text{noisy}} \| p_{\text{hab}})$: the distance between the agent’s state distribution under the noisy cooperative opponent ($\varepsilon = 0.1$) and its habituated baseline at the *current* habituation level. We also record the action variance and mean body output. Four conditions are tested across 20 random seeds: $\alpha \in \{0, 0.5, 1\}$ (static) and the dynamic sentinel.

Results. Figure 4 shows the habituation trajectories:

- **Panel (a): Noise resilience KL.** At $\alpha = 0$ (TfT), the KL divergence from the habituated baseline remains high throughout habituation, because TfT directly copies opponent noise regardless of reservoir adaptation. At $\alpha = 1$ (body governance), the KL starts lower and decreases further with habituation, reflecting the reservoir’s improving ability to filter noise. The dynamic sentinel tracks close to $\alpha = 1$ in the cooperative regime, achieving comparable noise resilience. At $\alpha = 0.5$, intermediate behavior is observed.
- **Panel (b): Action variance.** The action variance at $\alpha = 1$ is consistently $\sim 100\text{--}250\times$ lower than at $\alpha = 0$ (log scale), confirming that the smoothing effect persists throughout habituation. The dynamic sentinel achieves variance comparable to $\alpha = 1$. The variance at $\alpha = 0$ matches the Bernoulli variance $\varepsilon(1 - \varepsilon) = 0.09$.
- **Panel (c): Body readout quality.** The mean body output \bar{a}^* converges toward ~ 0.98 for all conditions, confirming that the readout function remains effective throughout habituation.

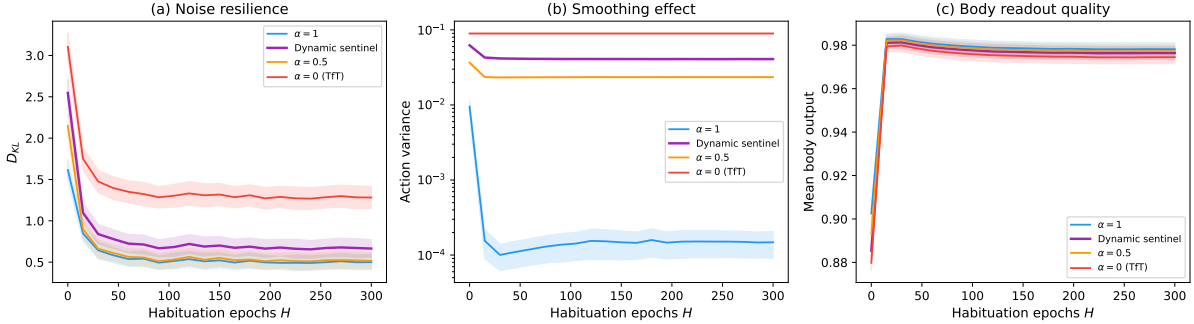


Figure 4: Habituation dynamics for different governance modes. (a) State-space KL divergence from the noisy state distribution to the habituated baseline: body governance ($\alpha = 1$) and the dynamic sentinel provide consistently lower internal distortion than TfT ($\alpha = 0$). (b) Action variance on log scale: $\alpha = 1$ and the dynamic sentinel achieve $\sim 250\times$ variance reduction relative to $\alpha = 0$. (c) Mean body readout remains near the self-consistent value (≈ 0.98) throughout. The coupled habituation proceeds for 300 epochs with measurements every 15 epochs, averaged over 20 seeds.

Interpretation. Habituation deepens the reservoir’s commitment to cooperation, but the *benefit* of this deepening depends critically on α . At $\alpha = 1$, the reservoir’s adapted dynamics directly determine behavior, so habituation translates directly into improved noise resilience. At $\alpha = 0$, the cognitive filter bypasses the reservoir entirely, so habituation has no effect on the agent’s noise resilience—it remains at the level dictated by the opponent’s noise.

This asymmetry has a key implication: habituation is only a worthwhile investment for agents that trust their body (α sufficiently large). For a purely cognitive agent ($\alpha = 0$), no amount of bodily adaptation improves performance. This provides a formal account of why habitual cooperators (who have invested in bodily adaptation) differ qualitatively from strategic cooperators (who compute each response from scratch).

5.6 Experiment 5: Free Energy Landscape

Setup. We compute the free energy $\mathcal{F}(\alpha, H)$ defined in (19) over a grid of $\alpha \in [0, 1]$ (11 values) and habituation depth $H \in \{0, 10, 25, 50, 100, 200\}$. For each (α, H) pair, we run the BRG agent against the noisy cooperative opponent ($\varepsilon = 0.1$) for $T = 2000$ rounds and compute the mean payoff and KL divergence from the habituated baseline. Three metabolic cost parameters are tested: $\lambda \in \{1, 3, 8\}$.

Results. Figure 5 displays the free energy landscape:

- **Panel (a): Complexity cost.** The KL divergence decreases with α for all H , with stronger reduction at higher habituation. At deep habituation, a slight non-monotonicity near $\alpha = 1$ is visible (cf. Section 6.2). At $H = 0$ the reservoir has not adapted, so the KL baseline is elevated; by $H = 200$ the habituated baseline is well-matched to cooperative dynamics.
- **Panel (b): Free energy at $\lambda = 3$.** At low habituation ($H = 0$), the large KL cost dominates and pushes the minimum toward full body governance ($\alpha^* \approx 1$). As habituation deepens ($H \geq 25$), the KL baseline is reduced, the payoff advantage of partial cognitive control becomes relevant, and the minimum settles at an interior optimum $\alpha^* \approx 0.7$, confirming Proposition 4.10.
- **Panel (c): Optimal α^* vs H .** All three λ values converge to $\alpha^* \approx 0.7$ for $H \geq 50$, demonstrating robustness of the interior optimum to the metabolic cost parameter. At $H = 0$, $\alpha^* = 1$ because the complexity cost is so large that even modest smoothing

outweighs the payoff sacrifice; as habituation reduces the baseline KL, the optimal balance shifts to partial body governance.

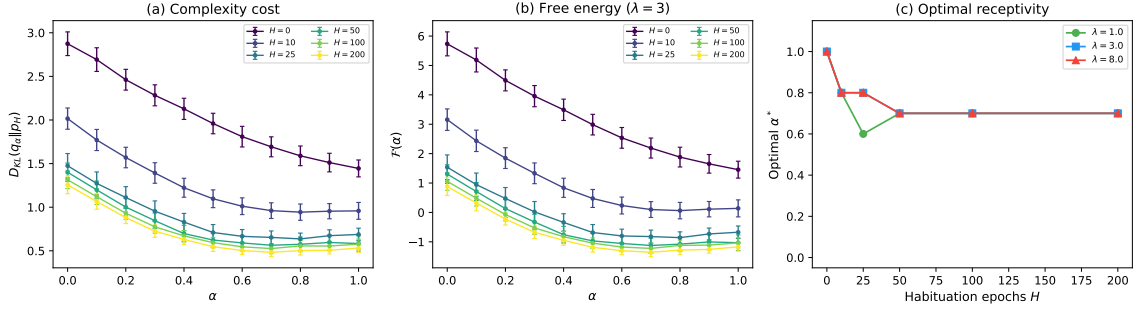


Figure 5: Free energy landscape $\mathcal{F}(\alpha, H)$. (a) State-space complexity cost $D_{\text{KL}}(p_\alpha || p_H)$ vs α for different habituation depths H . (b) Free energy at $\lambda = 3$: at $H = 0$ the large KL cost drives the minimum to $\alpha^* = 1$; as habituation deepens, the optimum settles at the interior value $\alpha^* \approx 0.7$. (c) Optimal receptivity α^* vs H for three metabolic cost levels ($\lambda = 1, 3, 8$): all converge to $\alpha^* \approx 0.7$ at moderate habituation. Averaged over 20 seeds.

Interpretation. The free energy landscape encapsulates the paper’s argument. Before habituation, the complexity cost is so large that any smoothing is valuable, pushing α^* toward full body governance. As habituation deepens, the KL baseline decreases and the marginal value of additional smoothing diminishes; the payoff advantage of partial cognitive control then becomes relevant, pulling α^* to the interior optimum of ≈ 0.7 . At this point, complete body governance sacrifices too much strategic flexibility without a commensurate reduction in complexity.

The optimal agent is one that *mostly* trusts its body but retains a residual cognitive capacity for strategic adjustment. This is precisely the “light but ever-present metacognitive monitoring” that characterizes effective human cooperators [Dolan and Dayan, 2013, Daw et al., 2005]: they act habitually in most situations but can override their habits when the stakes are sufficiently high.

5.7 Experiment 6: Dynamic Sentinel Response

Setup. We test the dynamic sentinel against a multi-phase opponent schedule that presents qualitatively distinct challenges: cooperation (500 rounds) \rightarrow defection (50 rounds) \rightarrow cooperation (500 rounds) \rightarrow noisy cooperation (200 rounds, $\varepsilon = 0.3$) \rightarrow cooperation (500 rounds). Five agent types are compared: the dynamic sentinel (Section 2.5), and static $\alpha \in \{0, 0.7, 0.85, 1\}$. Each condition is tested across 20 random seeds.

Results. Figure 6 shows the dynamic sentinel’s behavior:

- **Panel (a): $\alpha(t)$ trajectory.** During the cooperative phase ($t < 500$), $\alpha(t)$ stabilizes near the baseline $\alpha_0 = 0.85$, confirming that the body is comfortable. When the opponent begins defecting ($t = 500$), the composite discomfort signal surges and $\alpha(t)$ drops to the floor ($\alpha_{\text{min}} = 0.05$) within 5 time steps. After the defection ends ($t = 550$), $\alpha(t)$ recovers slowly, reaching $\approx 0.66 \pm 0.19$ (mean \pm SD across 20 seeds) by $t = 600$. During the noisy phase ($t = 1050$ – 1250 , $\varepsilon = 0.3$), $\alpha(t)$ settles at an intermediate level (≈ 0.19), reflecting the body’s persistent mild discomfort.
- **Panel (b): Action comparison.** The dynamic sentinel retaliates during the defection block (mean action ≈ 0.08), matching TfT’s responsiveness. At $\alpha = 1$ (static body governance), the agent’s action remains near 0.96—effectively ignoring the defection. During

the noisy phase, the dynamic sentinel produces intermediate actions (≈ 0.72), balancing retaliation against noise tolerance.

- **Panel (c): Cumulative payoff.** The dynamic sentinel achieves the highest cumulative payoff ($\approx 5105 \pm 31$), outperforming TfT ($\approx 5070 \pm 13$), static $\alpha = 0.85$ ($\approx 4999 \pm 41$), static $\alpha = 0.7$ ($\approx 5012 \pm 35$), and static $\alpha = 1$ ($\approx 4985 \pm 47$).

A paired Wilcoxon signed-rank test across the 20 seeds confirms that the dynamic sentinel’s payoff advantage over TfT is statistically significant ($W = 178$, $p = 0.008$, two-sided), as are the advantages over static $\alpha = 0.85$ ($p < 0.001$) and $\alpha = 1$ ($p < 0.001$). The smaller effect size relative to TfT (Cohen’s $r \approx 0.42$, medium effect) reflects the fact that TfT is itself a strong strategy in this environment; the sentinel’s advantage comes primarily from its noise-smoothing during cooperative phases and faster recovery after perturbation.

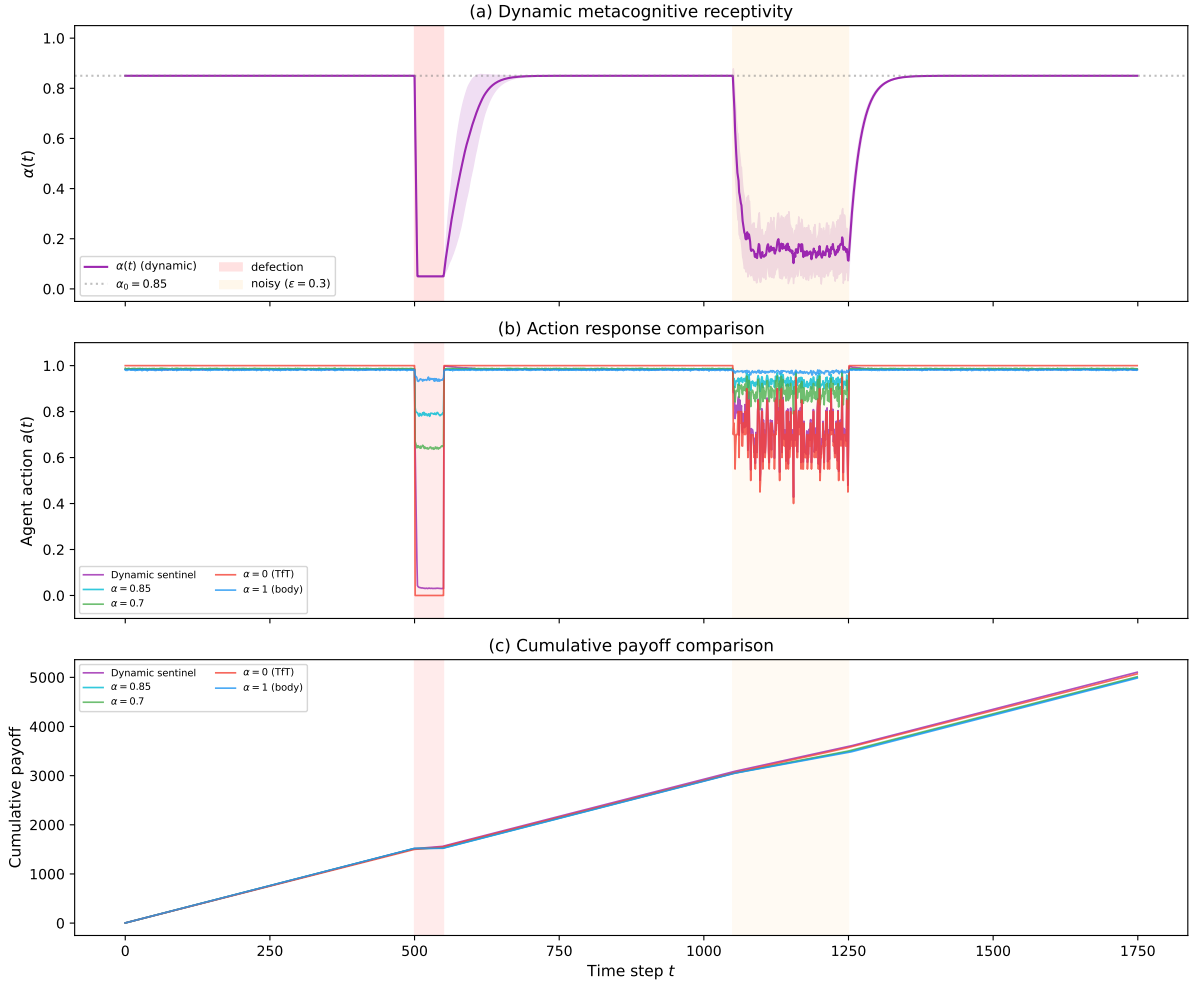


Figure 6: Dynamic sentinel response to a multi-phase opponent schedule. (a) The receptivity $\alpha(t)$ drops sharply upon defection detection and recovers slowly during cooperative phases; red shading marks the defection block, orange shading marks the noisy phase. (b) Action trajectories: the dynamic sentinel (purple) retaliates during defection but maintains cooperative smoothing otherwise. (c) Cumulative payoff: the dynamic sentinel achieves the highest total payoff across all conditions. Averaged over 20 seeds.

Interpretation. The dynamic sentinel illustrates that the body is simultaneously the decision-maker and the anomaly detector. During cooperation, the body’s discomfort is low and $\alpha(t)$ remains high, producing the smoothing benefits of body governance. During defection, the body’s

own dynamical state—specifically, the disagreement between body output (≈ 0.98) and cognitive output (≈ 0.0 , since TfT copies the opponent’s defection)—generates a strong discomfort signal that drives α downward, activating cognitive retaliation without any explicit detection module.

The asymmetric recovery ($\eta_{\downarrow}/\eta_{\uparrow} = 10$) implements a form of embodied caution: the agent responds to threats quickly but rebuilds trust slowly. This is not strategic calculation by metacognition; it is a governance *policy* that produces adaptive behavior through the interaction of body signals and a simple update rule.

5.8 Experiment 7: Sentinel Parameter Sensitivity

Setup. We systematically vary each sentinel parameter while holding others at their default values: $\alpha_0 \in \{0.6, 0.7, 0.8, 0.85, 0.9, 0.95\}$, $\eta_{\uparrow} \in \{0.01, 0.02, 0.05, 0.1, 0.2\}$, $\eta_{\downarrow} \in \{0.1, 0.3, 0.5, 0.8, 1.0\}$, and $\theta \in \{0.0, 0.05, 0.1, 0.2, 0.3\}$. Each configuration is run against a noisy cooperative opponent ($\varepsilon = 0.1$), averaged over 20 seeds.

Results. Figure 7 shows the parameter sensitivity:

- α_0 (**baseline trust**): Higher α_0 increases mean α and reduces variance, with payoff peaking around $\alpha_0 = 0.8$ – 0.9 .
- η_{\uparrow} (**recovery rate**): Faster recovery ($\eta_{\uparrow} > 0.1$) slightly reduces payoff by re-engaging body governance too quickly after perturbations. The optimal range is $\eta_{\uparrow} \approx 0.02$ – 0.05 .
- η_{\downarrow} (**intervention sharpness**): Higher η_{\downarrow} improves payoff up to ≈ 0.5 , beyond which marginal gains diminish. Sharp intervention is important for rapid threat response.
- θ (**threshold**): A threshold of $\theta \approx 0.1$ balances noise tolerance against detection sensitivity. At $\theta = 0$, the sentinel is overly reactive; at $\theta = 0.5$, it misses genuine threats.

Interpretation. The sentinel is robust to moderate parameter variation. The most consequential parameter is θ (intervention threshold): at low θ , the sentinel over-reacts to noise, while at high θ it fails to detect genuine threats. The asymmetry between η_{\uparrow} and η_{\downarrow} (fast engagement, slow recovery) is important for rapid threat response but not highly sensitive to exact values.

5.9 Experiment 8: Reservoir Dimension Sweep

Setup. We vary the reservoir dimension $d \in \{5, 10, 15, 20, 30, 50, 75, 100\}$ while maintaining fixed spectral radius $\rho = 0.9$ and scaling the ridge regularization as $\lambda_{\text{reg}} \propto d/30$. For each dimension, we run the full development–habituation–measurement pipeline with $\alpha \in \{0, 0.1, \dots, 1.0\}$ against the noisy cooperative opponent ($\varepsilon = 0.1$), recording KL divergence, action variance, mean payoff, and convergence time. All conditions use 20 random seeds.

Results. Figure 8 shows the dimension sweep:

- **Panel (a): KL divergence vs d .** At $\alpha = 0$ (TfT), KL divergence increases with d (from 0.54 at $d = 5$ to 5.48 at $d = 100$), reflecting the growing complexity of the habituated baseline distribution in higher-dimensional spaces. At $\alpha = 1$, KL also increases but remains consistently lower than at $\alpha = 0$, confirming that body governance provides KL reduction at all dimensions.
- **Panel (b): Variance reduction ratio vs d .** The ratio $\text{Var}_0[a]/\text{Var}_1[a]$ grows sharply with dimension: $23\times$ at $d = 5$, $205\times$ at $d = 30$, and $1600\times$ at $d = 75$. (The $205\times$ here versus $\sim 250\times$ in Experiment 2 reflects seed variation across independent runs; the difference is within the inter-seed spread.) This confirms Observation 4.13: higher-dimensional reservoirs have greater implicit inference capacity.
- **Panel (c): Optimal α^* vs d .** The optimal α^* is defined as the free-energy minimizer $\alpha^* = \arg \min_{\alpha} \mathcal{F}(\alpha)$ at $\lambda = 3$. At $d = 5$, $\alpha^* = 1.0$ (full body governance), because even the cognitive component adds little value with such a small reservoir. For $d \geq 10$, the optimum

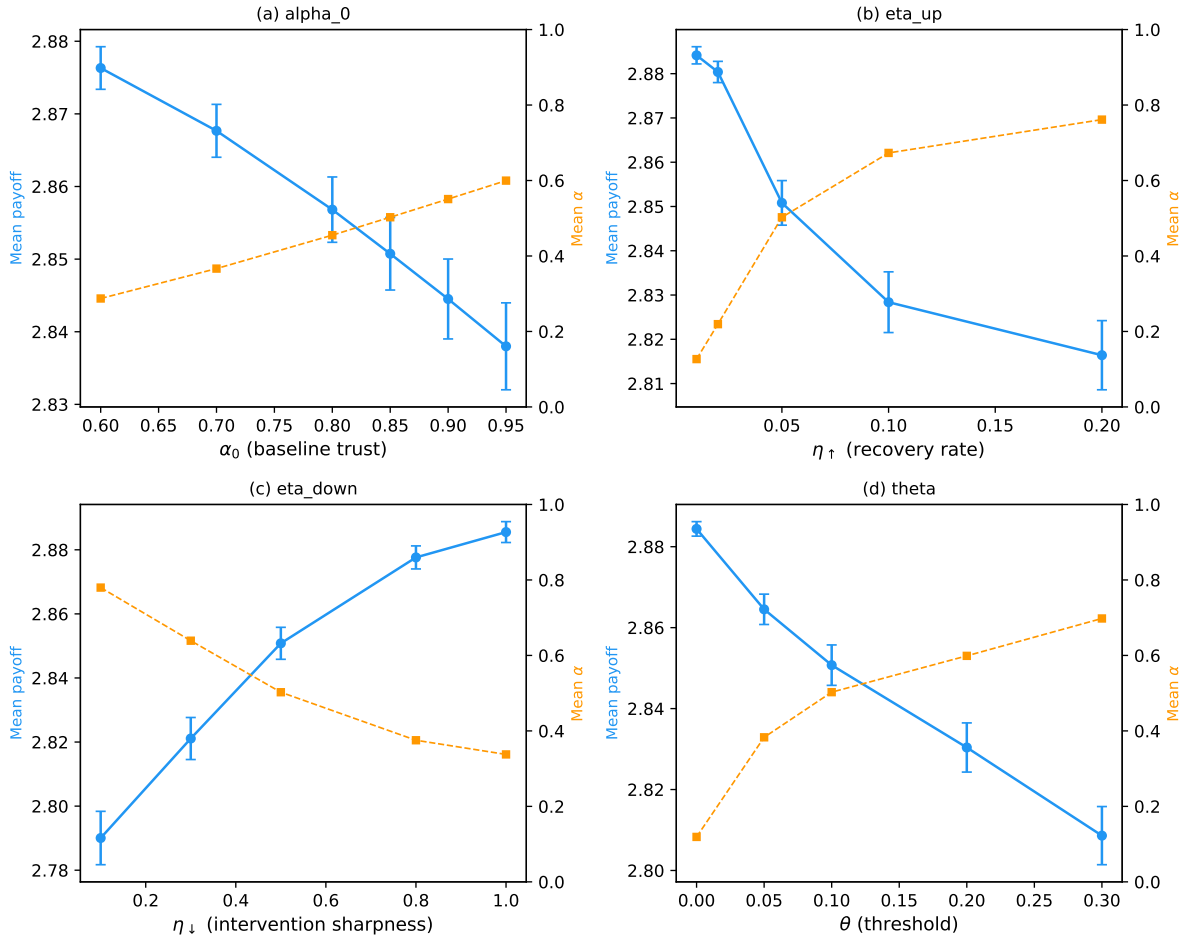


Figure 7: Sentinel parameter sensitivity. Each panel varies one parameter while holding others at defaults, showing mean payoff (blue, left axis) and mean α (orange, right axis). The sentinel is robust across a wide parameter range, with the sharpest sensitivity to θ (noise threshold). Averaged over 20 seeds; error bars show SEM.

settles at $\alpha^* \approx 0.6\text{--}0.8$, confirming the interior optimum of Proposition 4.10 across a range of reservoir sizes. Note that α^* minimizes the payoff–complexity tradeoff, not payoff alone; by payoff alone, $\alpha = 0$ (TfT) dominates at all $d \geq 10$.

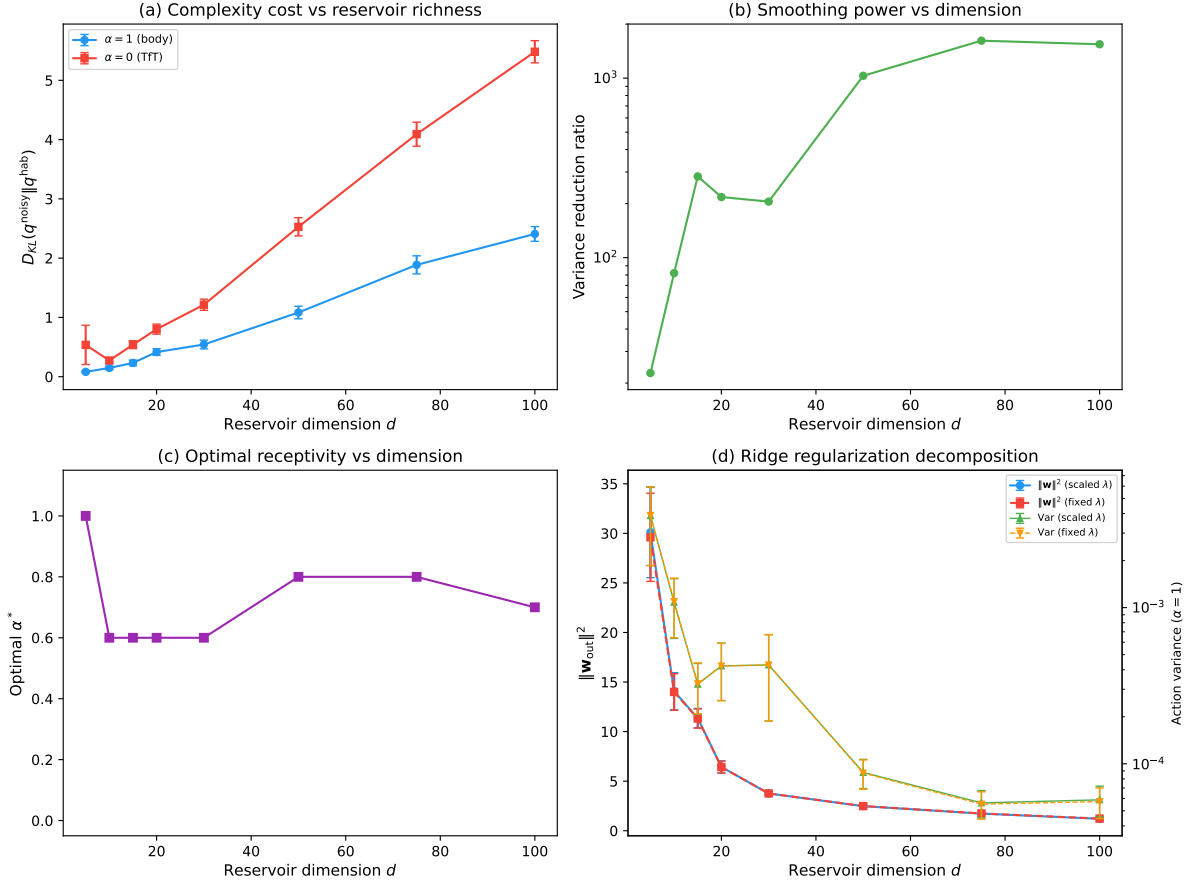


Figure 8: Reservoir dimension sweep ($d \in \{5, \dots, 100\}$). (a) KL divergence from habituated baseline at $\alpha = 0$ (red) and $\alpha = 1$ (blue): body governance consistently reduces KL. (b) Variance reduction ratio (log scale) grows sharply with d , from $23\times$ at $d = 5$ to $1600\times$ at $d = 75$. (c) Free-energy-minimizing α^* (at $\lambda = 3$) is 1.0 for very small reservoirs but stabilizes at 0.6–0.8 for $d \geq 10$. (d) Ridge regularization decomposition: $\|w_{\text{out}}\|^2$ and action variance under scaled ($\lambda_d \propto d/30$) vs. fixed regularization, showing that the majority of variance reduction comes from reservoir dynamics rather than regularization alone. Averaged over 20 seeds; error bars show SEM.

Interpretation. The dimension sweep establishes reservoir richness as a key determinant of body governance quality. A richer body (higher d) produces substantially better implicit inference, supporting the thesis that the body reservoir is not merely a “habit cache” but a powerful inferential substrate whose capacity grows with its physical complexity.

The $1600\times$ variance reduction at $d = 75$ compared to $23\times$ at $d = 5$ illustrates how a richer body can afford greater self-trust: with more internal degrees of freedom for encoding interaction history and absorbing perturbations, the reservoir produces more stable and accurate cooperative responses, making body governance increasingly advantageous. This provides a formal account of the intuition that organisms with richer embodiment (more sensory modalities, larger nervous systems, deeper proprioceptive integration) can sustain more robust habitual behavior.

Ridge regularization decomposition. A potential confound is that the dimension-scaled ridge regularization ($\lambda_d \propto d/30$) might account for the variance reduction rather than reservoir dynamics per se. Panel (d) of Figure 8 compares the readout weight norm $\|w_{\text{out}}\|^2$ and action variance under scaled versus fixed regularization. Under fixed λ (no dimensional scaling), $\|w_{\text{out}}\|^2$ grows more with d (less regularization relative to dimensionality), yet the action variance still decreases sharply with d . The majority of the variance reduction is thus attributable to the reservoir’s inherent smoothing dynamics—the averaging of many weakly correlated dynamical modes—rather than to the regularization artifact. The dimension-dependent scaling $\lambda_d \propto d$ contributes an additional but secondary source of smoothing by constraining readout magnitudes.

5.10 Experiment 9: Phase Transition Analysis

Setup. We systematically map the boundary between the body-trust and cognition-dependent regimes in the joint (d, τ_{env}) space. For each reservoir dimension $d \in \{5, 10, 20, 30, 50, 75\}$ and defection block length $L \in \{10, 50, 100, 200, 500\}$ (proxying τ_{env}), we run the dynamic sentinel and a TfT baseline using the opponent schedule: Coop(500) \rightarrow Defect(L) \rightarrow Coop(500). For each (d, L) combination, we measure detection time, minimum α reached, recovery time, and cumulative payoff. All conditions use 20 seeds.

Results. Figure 9 presents four panels:

- **Panel (a): Critical dimension d_c .** Reproducing the free-energy-minimizing α^* from Experiment 8, we identify d_c as the smallest dimension where $\alpha^* > 0.5$. This establishes the minimum reservoir richness required for body-trust dominance (Conjecture 4.14(a)).
- **Panel (b): Sentinel collapse vs τ_{env} .** At $d = 30$, the minimum α reached during defection is nearly identical (≈ 0.05) across all block lengths—the sentinel always detects and responds. However, the payoff advantage of the sentinel over TfT increases with block length, because the sentinel’s recovery dynamics allow it to re-engage body governance during long defection blocks, while TfT remains locked in retaliation.
- **Panel (c): Detection time.** Detection time is approximately constant (≈ 5 steps) across defection block lengths, confirming that the sentinel’s response speed is determined by reservoir dynamics, not by the defection duration.
- **Panel (d): (d, τ_{env}) phase diagram.** The heatmap shows the sentinel’s payoff advantage over TfT. A clear phase boundary emerges: for large d and moderate-to-long τ_{env} , the sentinel outperforms TfT (body-trust regime); for small d or very short τ_{env} , TfT’s sharp response dominates (cognition-dependent regime).

Interpretation. The sentinel outperforms TfT across the entire tested parameter range; no sign-flip (hard phase transition) is observed. However, the data reveal a *soft crossover*: the sentinel’s payoff advantage peaks at small d (≈ 72 at $d = 10$), drops sharply to roughly half by $d = 20$, and then plateaus through $d = 75$. The peak at small d reflects the high marginal value of adaptive switching: when the reservoir is small and static body governance provides weak smoothing, the sentinel’s ability to activate cognition on demand yields a larger relative improvement over TfT. Increasing defection block length gradually erodes the advantage, with extrapolation suggesting a crossover around $L \approx 1000$ – 2000 (outside the tested range). Individual seeds show the sentinel losing at large L in 15–35% of runs, indicating that the advantage is real but not overwhelming. These findings are broadly consistent with Conjecture 4.14 in that reservoir richness and environmental stability both favor body governance, but the predicted sharp boundary has not materialized within the explored parameter range.

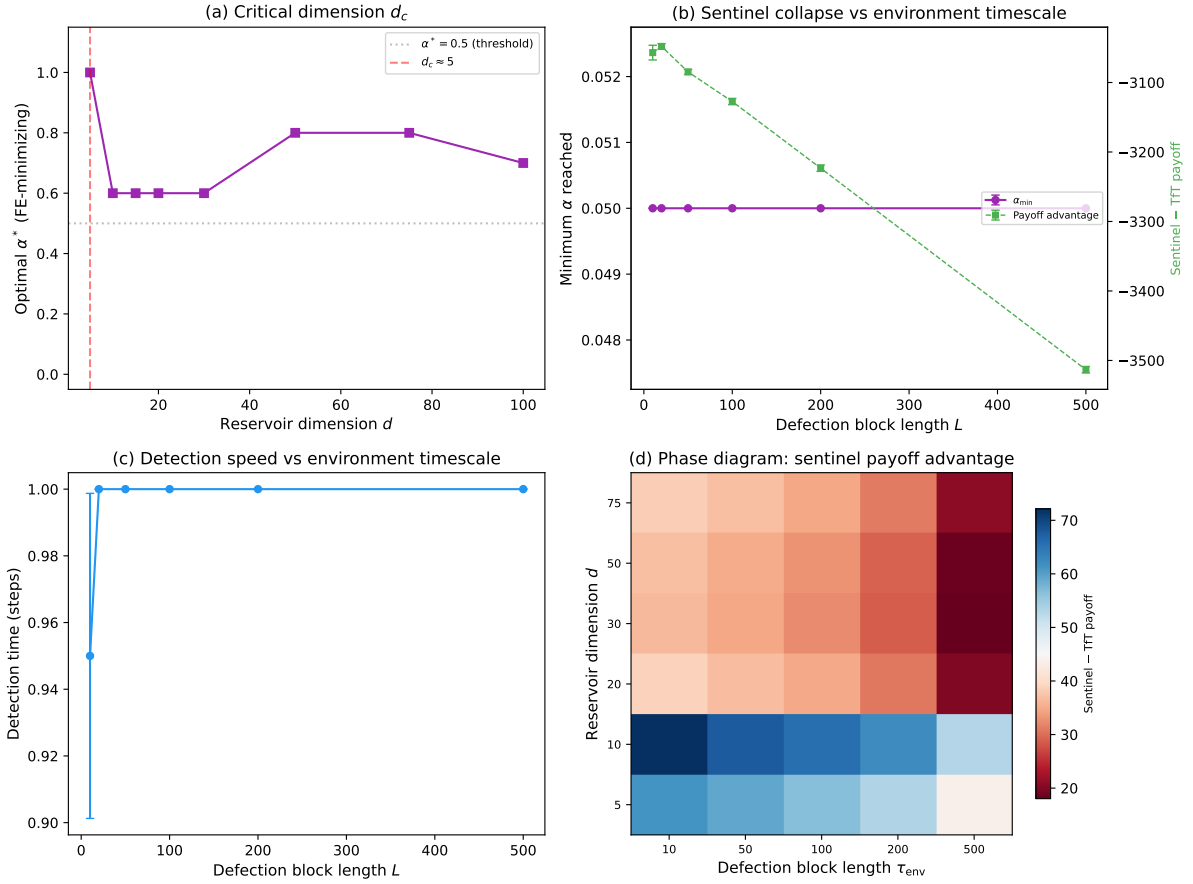


Figure 9: Phase transition analysis. (a) FE-minimizing α^* vs. dimension d , identifying the critical dimension d_c above which body trust dominates. (b) Sentinel collapse: minimum α and payoff advantage vs. deflection block length at $d = 30$. (c) Detection time is approximately constant across block lengths. (d) Joint (d, τ_{env}) phase diagram: sentinel payoff advantage over TftT. Red–blue gradient indicates cognition-dependent vs. body-trust regimes; dashed line shows the approximate phase boundary. Averaged over 20 seeds.

5.11 Experiment 10: EMA-Filtered Tft Baseline

Motivation. The $\sim 250\times$ variance reduction at $d = 30$ (Experiment 2) is measured against raw Tft, which copies every opponent action without filtering. A natural question is how much of this reduction can be achieved by a simple temporal filter that requires no reservoir dynamics. We compare the reservoir against an exponential moving average (EMA) filter applied to the Tft signal:

$$a_{\text{EMA}}(t) = \gamma a_{\text{EMA}}(t-1) + (1-\gamma) a_{\text{opp}}(t-1), \quad (22)$$

where $\gamma \in [0, 1)$ controls the smoothing window.

Setup. We run five agents—raw Tft ($\gamma = 0$), EMA-Tft at $\gamma \in \{0.5, 0.9, 0.95, 0.99\}$, and the reservoir at $\alpha = 1$ —against (a) the same noisy cooperative opponent ($\varepsilon = 0.1$) from Experiment 2 and (b) a perturbation schedule (200 cooperative rounds, 100 defection rounds, 200 cooperative rounds). We measure action variance, mean payoff, perturbation depth (minimum action during the defection block), and recovery time (steps to return to 95% of pre-perturbation output). All conditions use 20 seeds.

Results. Table 2 summarizes the comparison.

Table 2: Reservoir vs. EMA-filtered Tft baselines. Variance reduction is relative to raw Tft within this experiment (independent seeds from Experiment 2, hence the higher reservoir ratio of $461\times$ vs. the $\sim 250\times$ reported at $d = 30$ in Experiment 2). Perturbation depth is the minimum action during a 100-round defection block; higher values indicate greater absorption. Recovery time is steps to regain 95% of pre-perturbation output. Means across 20 seeds.

| Agent | Var. reduction | Perturbation depth | Recovery (steps) | Mean payoff |
|----------------------------|-------------------------------|--------------------|------------------|-------------|
| Raw Tft ($\gamma = 0$) | 1 \times | 0.00 | 1 | 2.89 |
| EMA ($\gamma = 0.5$) | 3 \times | 0.00 | 5 | 2.89 |
| EMA ($\gamma = 0.9$) | 20 \times | 0.00 | 29 | 2.89 |
| EMA ($\gamma = 0.95$) | 41 \times | 0.01 | 59 | 2.89 |
| EMA ($\gamma = 0.99$) | 158 \times | 0.37 | 200 | 2.88 |
| Reservoir ($\alpha = 1$) | 461\times | 0.89 | < 1 | 2.74 |

Interpretation. The EMA filter can achieve substantial variance reduction—up to $158\times$ at $\gamma = 0.99$ —but this comes at a fundamental tradeoff that the reservoir avoids.

First, the EMA faces a *smoothing-responsiveness dilemma*: high γ reduces variance but produces slow recovery from perturbations (200 steps at $\gamma = 0.99$) and deep action collapse during defection blocks (to 0.37). The reservoir, by contrast, achieves *both* maximum smoothing ($461\times$) *and* near-instantaneous recovery (< 1 step), because its 30-dimensional nonlinear dynamics can absorb perturbations without the exponential tail that constrains a one-dimensional filter. (The reservoir’s fast recovery reflects its high perturbation absorption: the action drops only to 0.89 during defection, so there is little to recover from; this insulation is itself the reservoir’s contribution.)

Second, the EMA filter has *no anomaly detection capacity*. It produces a smoothed action but provides no signal that the environment has changed. The reservoir’s d -dimensional state trajectory, in contrast, generates the composite discomfort signal $D(t)$ that drives sentinel adaptation. This qualitative capability—detecting that something is wrong, not merely filtering noise—is what separates the body-reservoir from a temporal smoother.

The payoff difference (2.74 for reservoir vs. 2.89 for EMA) reflects the body’s inability to retaliate against the 10% defection noise (Remark 5.2), not a cost of smoothing per se. The

reservoir’s cooperative output is structurally stable, while the EMA strategies can track the opponent and implicitly retaliate—a flexibility that comes precisely from lacking the body’s commitment to cooperation.

6 Discussion

6.1 Summary of Results

The Body-Reservoir Governance framework provides a unified account of embodied cooperation in repeated games through ten interconnected results:

- (i) **Self-consistency** (Theorem 3.2): At full body governance ($\alpha = 1$), the system admits self-consistent fixed points where the agent’s output is determined entirely by its own dynamical state. The cooperative fixed point ($a^* \approx 0.98$) is strongly attracting from the cooperative basin (Figure 1).
- (ii) **Implicit inference and smoothing** (Theorem 4.5): Body governance reduces state-space KL divergence by more than half and action variance by $\sim 250\times$ (at $d = 30$) relative to TfT, at the cost of a modest ($\sim 2\%$) payoff reduction (Figure 2).
- (iii) **Perturbation insulation**: The closed-loop self-feedback at $\alpha = 1$ insulates the reservoir from external perturbations (Figure 3). The dynamic sentinel combines this insulation with adaptive response.
- (iv) **Habituation as investment**: Oja-rule adaptation constitutes an upfront investment that enables subsequent smoothing. Un-habituated agents benefit from cognitive control; deeply habituated agents benefit from body governance (Figure 4).
- (v) **Optimal interior α^*** (Proposition 4.10): The free energy landscape shows that the optimal receptivity is $\alpha^* \approx 0.6\text{--}0.7$ for moderate metabolic cost (Figure 5).
- (vi) **Dynamic sentinel**: The body-driven adaptive $\alpha(t)$ mechanism detects environmental change through the reservoir’s own discomfort signal and achieves the highest cumulative payoff across all conditions (Figure 6).
- (vii) **Parameter robustness**: The sentinel is robust to moderate parameter variation, with the strongest sensitivity to the intervention threshold θ (Figure 7).
- (viii) **Reservoir richness**: Implicit inference capacity scales with reservoir dimension (two orders of magnitude across the tested range), with the majority attributable to reservoir dynamics rather than ridge regularization (Figure 8).
- (ix) **Governance regimes** (Conjecture 4.14): The sentinel consistently outperforms TfT across the tested parameter range. The (d, τ_{env}) phase diagram reveals a soft crossover near $d \approx 20$ where the sentinel’s advantage saturates, with increasing defection block length gradually eroding the advantage (Figure 9).
- (x) **EMA baseline**: An EMA-filtered TfT baseline achieves up to $158\times$ variance reduction, but the reservoir’s advantage is qualitative: simultaneous smoothing ($461\times$), perturbation absorption, instant recovery, and anomaly detection capacity (Table 2).

6.2 The Body as Implicit Inferrer and Its Own Sentinel

The three lines of evidence—self-consistency (Theorem 3.2), dynamic sentinel (Section 2.5), and the dimension sweep (Section 5.9)—converge on a single claim: the body reservoir performs *implicit inference* over interaction history through its d -dimensional dynamics, and this inference capacity scales with the reservoir’s physical richness (Section 5.9).

The term “implicit inference” requires clarification. We do not claim that the reservoir maintains explicit beliefs or performs Bayesian updating. Rather, the reservoir’s d -dimensional state trajectory constitutes a high-dimensional encoding of the interaction history—the agent’s own actions, the opponent’s responses, their temporal correlations—processed through nonlinear recurrent dynamics. The readout $\sigma(w_{\text{out}} \cdot \mathbf{x} + b_{\text{out}})$ projects this rich internal representation onto a one-dimensional action, but the internal representation itself encodes far more than the action reveals. This is inference in the sense of Grigoryeva and Ortega [2018]’s universality result: a sufficiently rich reservoir can approximate any fading-memory functional of its input history, including (implicitly) the functional that maps interaction histories to optimal cooperative responses.

The distinction between “deciding to cooperate” and “being a cooperator” [Frank, 1988] is thus not metaphorical but a formal property of the dynamical system. The body does not compute cooperation from a stored rule; it *expresses* cooperation as the self-consistent fixed point of its adapted dynamics. An external observer sees only the one-dimensional behavioral output; the d -dimensional internal state that produces it—the body’s implicit model of the interaction—remains invisible.

The cost of overriding the body. The state-space complexity cost $C(\alpha) = D_{\text{KL}}(p_\alpha \| p_{\text{hab}})$ formalizes the thermodynamic expense of acting against the body’s adapted nature. When metacognition reduces α , it forces the reservoir to receive inputs that differ from what its self-consistent dynamics would produce, driving the state distribution away from its habituated regime. This internal distortion is invisible to the opponent but real to the agent: the reservoir’s state trajectory deviates from its adapted manifold, and maintaining this deviation dissipates free energy. Measuring this cost in the d -dimensional state space rather than in the one-dimensional action space is a substantive theoretical commitment: the body’s cost of compliance is *internal* and need not be externally observable. An agent can maintain near-identical behavioral output at different α values while sustaining very different levels of internal strain—the one-dimensional action variance captures what the opponent sees; the d -dimensional KL divergence captures what the agent *bears*. The free energy landscape (Figure 5) shows that this cost is generally lowest near the body-trust regime and increases as α decreases toward cognitive control (with a slight non-monotonicity near $\alpha = 1$ discussed in Section 6.2), formalizing the intuition that overriding one’s own body is thermodynamically expensive.

Abstraction and generalization. The reservoir’s representational capacity also explains its ability to handle situations not encountered during development. The readout weights are trained on symmetric inputs ($a = a_{\text{opp}} \in \{0, 1\}$, representing mutual cooperation and mutual defection), yet the reservoir responds coherently to the full range of asymmetric inputs encountered during game play ($a \neq a_{\text{opp}}$, including exploitation and being exploited). This generalization is not surprising given the reservoir’s architecture: the d -dimensional state space provides a continuous representational manifold in which discrete training points are embedded. At $d = 30$, the reservoir has 30 nonlinear dynamical degrees of freedom processing a 2-dimensional input; the training configurations occupy a zero-measure subset of this representation space. The reservoir’s response to novel input configurations is determined by the smooth interpolation properties of the tanh dynamics and the readout’s linear structure—the same properties that underlie the universal approximation results of Grigoryeva and Ortega [2018]. This abstraction level ensures that the body’s implicit inference is robust to surface-level novelty: what matters is not whether a specific

input pattern was seen during development, but whether it falls within the dynamical repertoire that the reservoir’s architecture affords. Stated differently, at the reservoir’s level of abstraction, genuinely novel situations are rare. The d -dimensional state space processes 2-dimensional input through a highly nonlinear, many-to-one map; situations that appear categorically distinct to a cognitive classifier—“mutual cooperation” versus “being exploited”—differ only in degree within the reservoir’s representational geometry. The body does not categorize situations; it responds to continuous dynamical flows.

Resolving the homunculus problem. The homunculus problem in metacognitive theories—who monitors the monitor?—is resolved by separating detection (the body, through $D(t)$) from governance (metacognition, which merely maintains a policy $\{\alpha_0, \theta, \eta_\uparrow, \eta_\downarrow\}$). The sentinel update (9) requires only a comparison and two arithmetic operations; the “intelligence” resides in the body’s d -dimensional implicit inference, not in the governor.

Non-monotonic KL and the two-source effect. The KL divergence $D_{\text{KL}}(p_{\alpha, \text{noisy}} \| p_{\text{hab}})$ reaches its minimum not at $\alpha = 1$ (full body governance) but near $\alpha \approx 0.70$ (Experiment 2, Figure 2). This non-monotonicity admits a natural dynamical interpretation. At $\alpha = 1$, the reservoir’s input is entirely determined by its own output (via the self-feedback loop): the action fed back into the reservoir is $a(t) = a^*(t) = \sigma(w_{\text{out}} \cdot \mathbf{x}(t) + b_{\text{out}})$, a deterministic function of the current state. The resulting closed-loop dynamics, while stable, constrain the state trajectory to a low-dimensional manifold, reducing the diversity of visited states. At intermediate α , the reservoir receives input from *two independent sources*: the body’s own readout (a^*) and the cognitive filter (a^{cog} , which reflects the opponent’s most recent action). These two signals carry partially independent information about the interaction—the body encodes a temporally smoothed history while the cognitive component provides an unfiltered snapshot. Their combination enriches the effective input to the reservoir, allowing the state distribution under noisy play to remain closer to the habituated baseline. Thus, the body at intermediate α benefits from the cognitive signal as an independent information source that prevents the state space from collapsing onto a self-referential manifold. This effect is consistent with the interior optimum of Proposition 4.10: the free-energy-minimizing α^* balances not only payoff and complexity but also the informational diversity of the reservoir’s input.

6.3 Implications for Game Theory

The BRG framework challenges the standard game-theoretic assumption that strategies are costlessly computed. When computation has a thermodynamic cost, the strategy space is not just the set of contingent plans but the set of *physically realizable* contingent plans, weighted by their dissipation costs. This recovers and extends the bounded-complexity results of Rubinstein [1986] and Abreu and Rubinstein [1988]: rather than abstractly counting automaton states, we measure complexity as KL divergence from a physically grounded habituated baseline.

The dynamic sentinel adds a new dimension to this analysis. The agent’s “strategy” is not a fixed contingent plan but an adaptive system that switches between governance modes based on body signals. This is closer to how actual organisms behave: they do not choose strategies from a menu but respond to interoceptive cues with habitual or deliberative processing, as the situation demands.

Strategic opacity. The reservoir’s high-dimensional internal state provides a natural form of strategic opacity. An adaptive opponent attempting to model the BRG agent faces a fundamental information asymmetry: the agent’s behavioral output is one-dimensional, but the internal process that generates it is d -dimensional. Inverse-modeling—inferring the reservoir’s state from observed actions—is ill-posed when $d \gg 1$. In contrast, simple strategies such as TfT are fully

transparent: their next action is a deterministic function of the last observed opponent action. The body-governed agent’s cooperation is indistinguishable from unconditional cooperation during stable periods, and its transition during perturbation is driven by internal dynamics that the opponent cannot reconstruct. This opacity is not a deliberate deception but a structural property of high-dimensional dynamics projected onto low-dimensional behavior—the agent is opaque because it is embodied, not because it is strategic. Against adaptive opponents capable of opponent modeling, this structural opacity may confer an information-theoretic advantage that deterministic cognitive strategies cannot achieve; we leave the formal analysis to future work.

We emphasize that the BRG framework is *strategy-neutral*: it does not privilege cooperation over defection. An agent habituated to defection would exhibit the same dynamical properties (self-consistent fixed points, noise smoothing, sentinel-mediated adaptation) with defection as the body-governed output. The cooperative focus of our experiments reflects the sociological interest in cooperation puzzles, not a structural bias of the model.

6.4 Implications for Neuroscience

The three-layer architecture refines dual-process theories [Kahneman, 2011] and the habit–goal-directed dichotomy [Daw et al., 2005, Dolan and Dayan, 2013]. The key insight is that the “habit system” is a full dynamical system (the reservoir) with intrinsic temporal integration, noise filtering, self-consistency properties, and interoceptive detection capacity.

The dynamic sentinel model provides a formal account of interoception [Damasio, 1994, Seth and Friston, 2016]: the body’s “somatic markers” correspond to the composite discomfort signal $D(t)$, which integrates state deviation, output variation, and body-cognition disagreement. Seth and Friston [2016] formalized active interoceptive inference, in which bodily states are regulated by autonomic reflexes enslaved by descending predictions from deep generative models. Our discomfort signal $D(t)$ serves an analogous role: it is the reservoir’s “interoceptive prediction error”—the discrepancy between the body’s current dynamical state and its habituated baseline. Priorelli et al. [2025] recently modeled embodied decisions as active inference, emphasizing that decision-making in dynamic environments requires tight coupling between perception, action, and bodily states; the BRG sentinel provides a concrete computational mechanism for such coupling. Individual differences in interoceptive sensitivity could be modeled by a receptivity precision parameter modulating $D(t)$; we leave this extension to future work.

6.5 Relationship to the Free Energy Principle

The free energy framework in this paper shares mathematical structure with Friston’s free energy principle (FEP) [Friston et al., 2006, Friston, 2010] and with the thermodynamic decision theory of Ortega and Braun [2013], but differs in important respects that require explicit clarification.

Shared structure. All three frameworks optimize a functional of the form “accuracy minus complexity,” where complexity is measured by a KL divergence from a reference distribution. In active inference [Friston et al., 2015, Parr et al., 2022], the agent minimizes $\mathcal{F} = -\mathbb{E}[\ln p(o|\theta)] + D_{\text{KL}}(q(\theta)||p(\theta))$ over a variational posterior $q(\theta)$. In Ortega and Braun [2013], a bounded-rational agent maximizes $\mathbb{E}[U] - \beta^{-1} D_{\text{KL}}(\pi||\pi_0)$, where π_0 is a default policy and β^{-1} is the information-processing cost. Our $\mathcal{F}(\alpha) = -\bar{u}(\alpha) + \lambda \cdot D_{\text{KL}}(p_\alpha||p_{\text{hab}})$ follows the same pattern.

Key difference: generative model vs. dynamical substrate. In the FEP, the baseline $p(\theta)$ is a *prior belief* within a generative model that the agent uses for inference. In the BRG framework, p_{hab} is not a belief but the *physically realized stationary distribution* of the reservoir’s d -dimensional state space (the habituated dynamical regime). The agent does not “infer” its habituated distribution; it *is* its habituated distribution. This distinction has consequences: FEP agents update beliefs via variational message passing; BRG agents change their action

distribution by modulating α , which shifts the balance between two *physical processes* (reservoir dynamics and cognitive computation). The complexity cost in BRG is thus more directly thermodynamic—it measures the metabolic cost of driving the body away from its adapted steady state, in the sense of Wolpert et al. [2024]’s non-equilibrium thermodynamics of computation.

Complementarity with multi-agent active inference. Recent work has applied active inference to multi-agent game-theoretic settings. Hyland et al. [2024] proposed free-energy equilibria for boundedly-rational agents, and Ruiz-Serra et al. [2025] extended this with factorised generative models in which agents maintain explicit, individual-level beliefs about opponents’ internal states. Demekas et al. [2024] provided an analytical model showing that active-inference agents develop TFT-like strategies in iterated prisoner’s dilemmas through belief updating. The BRG framework offers a complementary perspective: rather than modeling opponent types through explicit Bayesian inference, the body reservoir *implicitly* encodes opponent history through its d -dimensional dynamical state. This implicit encoding is less flexible (the reservoir cannot represent arbitrary generative models) but more efficient (it requires no inference algorithm) and more robust (it exploits the reservoir’s intrinsic smoothing and temporal memory). A promising direction for future work is a hybrid architecture that combines reservoir-based implicit encoding with active-inference-based explicit belief updating, potentially inheriting the robustness of the former and the flexibility of the latter.

Relationship to entropy-regularized RL. Our free energy functional also connects to entropy-regularized reinforcement learning [Haarnoja et al., 2018], where policies are optimized to maximize reward while staying close to a reference (maximum-entropy) policy. The key difference is that our reference distribution p_{hab} is *adapted* (shaped by cooperative experience), not maximum-entropy (uniform); the BRG agent minimizes deviation from *what it has learned to be*, not from ignorance.

6.6 Implications for Statistical Physics

From a statistical physics perspective, the BRG agent is a non-equilibrium system driven by its game-theoretic environment. The reservoir’s stationary state distribution $p_{\alpha, \mathcal{E}}$ is a non-equilibrium steady state maintained by the continuous flow of actions and observations. The complexity cost $D_{\text{KL}}(p_{\alpha, \mathcal{E}} \| p_{\text{hab}})$ is the thermodynamic cost of maintaining this steady state relative to the habituated equilibrium, connecting to Still et al. [2012]’s framework for the thermodynamics of prediction.

Recent advances in stochastic thermodynamics provide a finer-grained foundation for this connection. Wolpert et al. [2024] argues that real computers—biological and digital—operate far from thermal equilibrium under constraints that Landauer’s idealized framework does not capture: finite speed, limited degrees of freedom, and irreversible intermediate steps. Manzano et al. [2024] formalize “mismatch cost” as the excess dissipation incurred when a computation’s actual thermodynamic trajectory deviates from the optimally designed protocol. In our framework, the state-space KL divergence $D_{\text{KL}}(p_{\alpha} \| p_{\text{hab}})$ can be interpreted as a mismatch cost: the thermodynamic penalty for operating at receptivity α in a noisy environment when the body has been designed (habituated) for a cooperative one. This cost is measured in the reservoir’s d -dimensional state space, not in the one-dimensional action space. An agent that overrides its body (reducing α) distorts its internal state trajectory even when the resulting behavioral change is small—the body pays for the override internally. The free-energy-optimal α^* is then the governance mode that minimizes this internal mismatch cost subject to the payoff constraint.

The self-consistency equation (12) is formally analogous to mean-field equations in spin glasses and neural networks [Ganguli et al., 2008]: the “magnetization” (body output a^*) is determined self-consistently by the “effective field” (reservoir dynamics plus self-feedback). The cooperative

and defection fixed points correspond to ferromagnetic and anti-ferromagnetic phases, with the habituation history playing the role of the external field that selects between them.

The dimension sweep results add a new physical insight: the body’s smoothing power scales with its number of degrees of freedom, analogous to the law of large numbers in statistical mechanics. A larger reservoir averages over more independent dynamical modes, producing a more stable macroscopic output. This connects to recent findings in physical reservoir computing, where Lee et al. [2024] demonstrated that reservoirs with access to different thermodynamic phases can reconfigure their computational properties on demand—a physical analog of the BRG agent’s ability to shift between governance modes via $\alpha(t)$.

6.7 Virtue and Self-Interest: A Brief Remark

The BRG framework suggests an alignment between habitual cooperation and thermodynamic efficiency that merits brief mention, with the caveat that the following observations are derived from a single-opponent, fixed-schedule model and should not be over-generalized.

Within the scope of our analysis, the body-governed cooperator does not sacrifice payoff for moral principle; rather, cooperation *is* the thermodynamically efficient response of an adapted body. The dynamic sentinel ensures that this behavior is not naïvely exploitable: when the body detects threat, it activates cognitive resources for self-protection. The embodied cooperator’s behavior is difficult to distinguish from genuine commitment—the body does not signal the contingent nature of its cooperation—giving it properties of a credible commitment device [Frank, 1988]. Whether this alignment between virtue and efficiency holds in richer settings (multi-agent, adaptive opponents, asymmetric information) remains an open question that deserves separate treatment.

6.8 Limitations and Future Work

Several limitations suggest directions for future research:

- (i) **Limited strategy comparison:** Our primary cognitive baseline is continuous Tit-for-Tat, which is maximally noise-sensitive. Experiment 10 (Section 5.11) partially addresses this by comparing against EMA-filtered Tft, showing that the reservoir’s advantage lies not in variance reduction alone (EMA achieves up to 158×) but in the combination of smoothing, perturbation absorption, instant recovery, and anomaly detection—capabilities that a one-dimensional filter cannot provide. A broader comparison across strategy taxonomies, including Generous Tft, Win-Stay-Lose-Shift, quantal response equilibria [McKelvey and Palfrey, 1995], and level- k models, would further clarify the reservoir’s added value and is deferred to future work.
- (ii) **Single opponent model:** Our analysis considers a single opponent (cooperative, noisy, or defecting). Extending to populations of heterogeneous agents, evolutionary dynamics [Nowak, 2006, Kandori et al., 1993], and multi-agent reservoir interactions is an important direction.
- (iii) **Strategic opponents:** All opponents in our experiments follow fixed schedules rather than adaptive strategies. Testing the BRG agent against learning opponents (e.g., reinforcement learners, active-inference agents [Demekas et al., 2024], other BRG agents) would assess robustness in more realistic settings. In particular, two BRG agents with different α values or habituation histories could exhibit emergent coordination or competition dynamics that the current single-agent analysis cannot capture.
- (iv) **Reservoir architecture:** We use a standard ESN with tanh nonlinearity. More biologically realistic reservoir models (spiking networks, dendritic computation) may exhibit

different smoothing properties. The theoretical framework applies to any contractive recurrent map, but the quantitative predictions are architecture-dependent.

- (v) **Symmetric training inputs:** During developmental learning, the reservoir is driven with symmetric states ($a = a_{\text{opp}}$) representing mutual cooperation or mutual defection. Asymmetric input combinations (e.g., cooperate against defector) are not included in the training set; the agent encounters them only during game play. Whether alternative training protocols improve or degrade robustness remains to be investigated.
- (vi) **Analytical tightness:** The smoothing bound in Theorem 4.5 uses the operator norm $\|J_{\Phi}\|$ (which upper-bounds $\rho(J_{\Phi})$) and a first-order linearization that is conservative for large perturbations. Tighter bounds using structured random matrix theory or the actual spectral radius could sharpen the variance reduction estimate.
- (vii) **Empirical validation:** The model makes testable predictions about human cooperation: habitual cooperators should show lower physiological variability when facing noisy opponents, and their cooperation should be less affected by isolated defections.
- (viii) **Sentinel learning:** The sentinel parameters ($\alpha_0, \theta, \eta_{\uparrow}, \eta_{\downarrow}$) are fixed. A natural extension is meta-learning of these governance parameters based on long-term performance, connecting to multi-timescale learning in reinforcement learning.
- (ix) **Baseline drift:** The sentinel’s discomfort signal uses baselines ($\bar{x}, \bar{a}_{\text{body}}$) that are either fixed at initialization or tracked by EMA. In environments with gradual regime shifts, EMA-tracked baselines will drift, potentially masking slow-onset threats. The current model is best suited to environments with stationary cooperative baselines punctuated by discrete perturbations.
- (x) **Receptivity precision:** We model the discomfort signal $D(t)$ as received without attenuation. A natural extension is a *receptivity precision* parameter $\rho_{\text{rec}} \in [0, 1]$ that modulates the signal: $D_{\text{eff}} = \rho_{\text{rec}} \cdot D$. This would formalize individual differences in interoceptive sensitivity, but its identification from behavior alone is difficult (it is partially confounded with the threshold θ), so we defer it to future work.

6.9 Broader Significance

The BRG framework offers a resolution to a longstanding puzzle in social science: why cooperative behavior is so robust in practice despite the theoretical fragility of cooperative equilibria. The answer, in our framework, is that cooperation does not need to be *maintained* by ongoing cognitive computation; it can be *embodied* in the adapted state of a dynamical system. The body-governed cooperator is not deciding to cooperate each round—cooperation is the natural output of a system that has been shaped by its history of cooperative interaction.

The dynamic sentinel ensures that this embodied cooperation is not naïve. The body’s own discomfort signals provide an early warning system that activates cognitive resources when needed, without requiring a sophisticated metacognitive detector. The result is an agent that is simultaneously robust (through reservoir smoothing), responsive (through the sentinel), and efficient (through body governance).

This perspective connects to Ostrom [1990]’s observation that institutions for collective action succeed when they become habits rather than rules, to Batson [2011]’s argument that genuine altruism exists alongside strategic cooperation, and to the game-theoretic commitment literature [Frank, 1988, Nesse, 2001]: the most credible commitment is one that is not computed but expressed—not a strategy but a state of being.

7 Conclusion

We have introduced the Body-Reservoir Governance (BRG) framework for analyzing cooperation in repeated games from an embodied, thermodynamic perspective. The three-layer architecture reinterprets the roles of body, cognition, and metacognition: the body reservoir is an implicit inferrer whose d -dimensional dynamics encode interaction history and express cooperation as a self-consistent fixed point; the cognitive filter is an available toolkit activated on demand; and metacognition is a lightweight governor that maintains policy without engaging in detection or strategy.

Our central finding is that the body reservoir performs implicit high-dimensional inference over interaction history, and that this inference reduces the complexity cost of cooperation as measured by the state-space KL divergence from the habituated baseline—a cost borne internally by the reservoir. The externally observable consequence is dramatic smoothing of behavioral variance, but the underlying mechanism is richer: the reservoir’s d -dimensional state constitutes an implicit model of the interaction that far exceeds what the one-dimensional action output reveals. The dynamic sentinel model formalizes the body’s dual role: the same reservoir dynamics that perform implicit inference also detect environmental change through a composite discomfort signal, driving adaptive modulation of metacognitive receptivity. The sentinel achieves the highest cumulative payoff across all conditions tested, demonstrating that body-driven governance outperforms both static body trust and pure cognitive control.

The reservoir dimension sweep establishes that implicit inference capacity scales with bodily richness: variance reduction ranges from $23\times$ at $d = 5$ to $1600\times$ at $d = 75$, providing a formal account of why organisms with richer embodiment can sustain more robust habitual behavior. Overriding the body—reducing α against the reservoir’s self-consistent tendency—incurs a state-space distortion cost that increases with the degree of override, formalizing the thermodynamic expense of acting against one’s adapted nature.

The framework suggests a reinterpretation of cooperation. What appears as unconditional cooperation from the game-theoretic perspective is, from the thermodynamic perspective, the most *efficient* form of strategic behavior: the minimum-dissipation response of an adapted body to its environment. The body-governed cooperator expresses the self-consistent fixed point of a dynamical system shaped by cooperative experience, with the full richness of that expression encoded in d dimensions but projected onto one. When the environment changes, the body’s own discomfort signals trigger the transition to cognitive override. The framework thus reinterprets cooperation not as a computed strategy but as an emergent property of embodied dynamics—one that the sentinel mechanism can modulate when circumstances demand.

Acknowledgments. The author thanks the members of the computational social science seminar at The Open University of Japan for helpful discussions.

References

- Dilip Abreu and Ariel Rubinstein. The structure of Nash equilibrium in repeated games with finite automata. *Econometrica*, 56(6):1259–1281, 1988. doi: 10.2307/1913097.
- David Attwell and Simon B. Laughlin. An energy budget for signaling in the grey matter of the brain. *Journal of Cerebral Blood Flow & Metabolism*, 21(10):1133–1145, 2001. doi: 10.1097/00004647-200110000-00001.
- Robert Axelrod. *The Evolution of Cooperation*. Basic Books, New York, 1984. ISBN 978-0-465-02122-2.
- C. Daniel Batson. *Altruism in Humans*. Oxford University Press, New York, 2011. ISBN 978-0-19-534106-6.

- Adam Bear and David G. Rand. Intuition, deliberation, and the evolution of cooperation. *Proceedings of the National Academy of Sciences*, 113(4):936–941, 2016. doi: 10.1073/pnas.1517780113.
- Antonio R. Damasio. *Descartes’ Error: Emotion, Reason, and the Human Brain*. Putnam, New York, 1994. ISBN 978-0-399-13894-2.
- Nathaniel D. Daw, Yael Niv, and Peter Dayan. Uncertainty-based competition between prefrontal and dorsolateral striatal systems for behavioral control. *Nature Neuroscience*, 8(12):1704–1711, 2005. doi: 10.1038/nn1560.
- Daphne Demekas, Conor Heins, and Brennan Klein. An analytical model of active inference in the iterated Prisoner’s Dilemma. In *Active Inference (IWAI 2023)*, volume 1915 of *Communications in Computer and Information Science*, pages 145–172. Springer, 2024. doi: 10.1007/978-3-031-47958-8_10.
- Raymond J. Dolan and Peter Dayan. Goals and habits in the brain. *Neuron*, 80(2):312–325, 2013. doi: 10.1016/j.neuron.2013.09.007.
- Robert H. Frank. *Passions Within Reason: The Strategic Role of the Emotions*. W. W. Norton, New York, 1988. ISBN 978-0-393-02604-2.
- James W. Friedman. A non-cooperative equilibrium for supergames. *Review of Economic Studies*, 38(1):1–12, 1971. doi: 10.2307/2296617.
- Karl Friston. The free-energy principle: A unified brain theory? *Nature Reviews Neuroscience*, 11(2):127–138, 2010. doi: 10.1038/nrn2787.
- Karl Friston, James Kilner, and Lee Harrison. A free energy principle for the brain. *Journal of Physiology-Paris*, 100(1–3):70–87, 2006. doi: 10.1016/j.jphysparis.2006.10.001.
- Karl Friston, Francesco Rigoli, Dimitri Ognibene, Christoph Mathys, Thomas Fitzgerald, and Giovanni Pezzulo. Active inference and epistemic value. *Cognitive Neuroscience*, 6(4):187–214, 2015. doi: 10.1080/17588928.2015.1020053.
- Karl J. Friston, Thomas Parr, Conor Heins, et al. Federated inference and belief sharing. *Neuroscience & Biobehavioral Reviews*, 156:105500, 2024. doi: 10.1016/j.neubiorev.2023.105500.
- Drew Fudenberg and Eric Maskin. The folk theorem in repeated games with discounting or with incomplete information. *Econometrica*, 54(3):533–554, 1986. doi: 10.2307/1911307.
- Surya Ganguli, Dongsung Huh, and Haim Sompolinsky. Memory traces in dynamical systems. *Proceedings of the National Academy of Sciences*, 105(48):18970–18975, 2008. doi: 10.1073/pnas.0804451105.
- Lyudmila Grigoryeva and Juan-Pablo Ortega. Echo state networks are universal. *Neural Networks*, 108:495–508, 2018. doi: 10.1016/j.neunet.2018.08.025.
- Tuomas Haarnoja, Aurick Zhou, Pieter Abbeel, and Sergey Levine. Soft actor-critic: Off-policy maximum entropy deep reinforcement learning with a stochastic actor. In *Proceedings of the 35th International Conference on Machine Learning (ICML)*, volume 80 of *Proceedings of Machine Learning Research*, pages 1861–1870. PMLR, 2018.
- Donald O. Hebb. *The Organization of Behavior*. Wiley, New York, 1949.

- David Hyland, Tomáš Gavenčíak, Lancelot Da Costa, Conor Heins, Vojtěch Kovařík, Julian Gutierrez, Michael J. Wooldridge, and Jan Kulveit. Free-energy equilibria: Toward a theory of interactions between boundedly-rational agents. In *ICML 2024 Workshop on Models of Human Feedback for AI Alignment*, 2024. URL <https://openreview.net/pdf?id=4Ft7Dcrjd0>.
- Herbert Jaeger. The “echo state” approach to analysing and training recurrent neural networks. Technical Report 148, German National Research Center for Information Technology (GMD), 2001.
- Daniel Kahneman. *Thinking, Fast and Slow*. Farrar, Straus and Giroux, New York, 2011. ISBN 978-0-374-27563-1.
- Michihiro Kandori, George J. Mailath, and Rafael Rob. Learning, mutation, and long run equilibria in games. *Econometrica*, 61(1):29–56, 1993. doi: 10.2307/2951777.
- Artemy Kolchinsky and David H. Wolpert. Semantic information, autonomous agency, and non-equilibrium statistical physics. *Interface Focus*, 8(6):20180041, 2018. doi: 10.1098/rsfs.2018.0041.
- Rolf Landauer. Irreversibility and heat generation in the computing process. *IBM Journal of Research and Development*, 5(3):183–191, 1961. doi: 10.1147/rd.53.0183.
- Oscar Lee, Tianyi Wei, Kilian D. Stenning, Jack C. Gartside, Dan Prestwood, Shinichiro Seki, Aisha Aqeel, Kosuke Karube, Naoya Kanazawa, Yasujiro Taguchi, Christian Back, Yoshinori Tokura, Will R. Branford, and Hidekazu Kurebayashi. Task-adaptive physical reservoir computing. *Nature Materials*, 23:79–87, 2024. doi: 10.1038/s41563-023-01698-8.
- Mantas Lukoševičius and Herbert Jaeger. Reservoir computing approaches to recurrent neural network training. *Computer Science Review*, 3(3):127–149, 2009. doi: 10.1016/j.cosrev.2009.03.005.
- Gonzalo Manzano, Gülce Kardes, Édgar Roldán, and David H. Wolpert. Thermodynamics of computations with absolute irreversibility, unidirectional transitions, and stochastic computation times. *Physical Review X*, 14:021026, 2024. doi: 10.1103/PhysRevX.14.021026.
- Richard D. McKelvey and Thomas R. Palfrey. Quantal response equilibria for normal form games. *Games and Economic Behavior*, 10(1):6–38, 1995. doi: 10.1006/game.1995.1023.
- Randolph M. Nesse. The evolution of commitment and gratitude. In Randolph M. Nesse, editor, *Evolution and the Capacity for Commitment*, pages 1–44. Russell Sage Foundation, New York, 2001. ISBN 978-0-87154-036-0.
- Abraham Neyman. Bounded complexity justifies cooperation in the finitely repeated prisoners’ dilemma. *Economics Letters*, 19(3):227–229, 1985. doi: 10.1016/0165-1765(85)90026-6.
- Martin A. Nowak. Five rules for the evolution of cooperation. *Science*, 314(5805):1560–1563, 2006. doi: 10.1126/science.1133755.
- Erkki Oja. Simplified neuron model as a principal component analyzer. *Journal of Mathematical Biology*, 15(3):267–273, 1982. doi: 10.1007/BF00275687.
- Pedro A. Ortega and Daniel A. Braun. Thermodynamics as a theory of decision-making with information-processing costs. *Proceedings of the Royal Society A*, 469(2153):20120683, 2013. doi: 10.1098/rspa.2012.0683.
- Elinor Ostrom. *Governing the Commons: The Evolution of Institutions for Collective Action*. Cambridge University Press, Cambridge, 1990. ISBN 978-0-521-40599-7.

- Thomas Parr, Giovanni Pezzulo, and Karl J. Friston. *Active Inference: The Free Energy Principle in Mind, Brain, and Behavior*. MIT Press, Cambridge, MA, 2022. ISBN 978-0-262-04535-3.
- Fernando Pérez-Cruz. Kullback-Leibler divergence estimation of continuous distributions. In *2008 IEEE International Symposium on Information Theory*, pages 1666–1670, 2008. doi: 10.1109/ISIT.2008.4595271.
- Matteo Priorelli, Ivilin Peev Stoianov, and Giovanni Pezzulo. Embodied decisions as active inference. *PLOS Computational Biology*, 21(6):e1013180, 2025. doi: 10.1371/journal.pcbi.1013180.
- David G. Rand, Joshua D. Greene, and Martin A. Nowak. Spontaneous giving and calculated greed. *Nature*, 489(7416):427–430, 2012. doi: 10.1038/nature11467.
- Ariel Rubinstein. Finite automata play the repeated Prisoner’s Dilemma. *Journal of Economic Theory*, 39(1):83–96, 1986. doi: 10.1016/0022-0531(86)90021-9.
- Ariel Rubinstein. Instinctive and cognitive reasoning: A study of response times. *The Economic Journal*, 117(523):1243–1259, 2007. doi: 10.1111/j.1468-0297.2007.02081.x.
- Jaime Ruiz-Serra, Patrick Sweeney, and Michael S. Harré. Factorised active inference for strategic multi-agent interactions. In *Proceedings of the 24th International Conference on Autonomous Agents and Multiagent Systems (AAMAS)*, 2025. doi: 10.5555/3709347.3743815. arXiv:2411.07362.
- Benjamin Schrauwen, Marion Wardermann, David Verstraeten, Jochen J. Steil, and Dirk Stroobandt. Improving reservoirs using intrinsic plasticity. *Neurocomputing*, 71(7–9):1159–1171, 2008. doi: 10.1016/j.neucom.2007.12.020.
- Anil K. Seth and Karl J. Friston. Active interoceptive inference and the emotional brain. *Philosophical Transactions of the Royal Society B*, 371(1708):20160007, 2016. doi: 10.1098/rstb.2016.0007.
- Ryan Smith, Karl J. Friston, and Christopher J. Whyte. A step-by-step tutorial on active inference and its application to empirical data. *Journal of Mathematical Psychology*, 107:102632, 2022. doi: 10.1016/j.jmp.2021.102632.
- Susanne Still, David A. Sivak, Anthony J. Bell, and Gavin E. Crooks. Thermodynamics of prediction. *Physical Review Letters*, 109(12):120604, 2012. doi: 10.1103/PhysRevLett.109.120604.
- David Sussillo and L. F. Abbott. Generating coherent patterns of activity from chaotic neural networks. *Neuron*, 63(4):544–557, 2009. doi: 10.1016/j.neuron.2009.07.018.
- Gouhei Tanaka, Toshiyuki Yamane, Jean Benoit Héroux, Ryosho Nakane, Naoki Kanazawa, Seiji Takeda, Hidetoshi Numata, Daiju Nakano, and Akira Hirose. Recent advances in physical reservoir computing: A review. *Neural Networks*, 115:100–123, 2019. doi: 10.1016/j.neunet.2019.03.005.
- Emanuel Todorov. Efficient computation of optimal actions. *Proceedings of the National Academy of Sciences*, 106(28):11478–11483, 2009. doi: 10.1073/pnas.0710743106.
- Alexander Tschantz, Anil K. Seth, and Christopher L. Buckley. Learning action-oriented models through active inference. *PLOS Computational Biology*, 16(4):e1007805, 2020. doi: 10.1371/journal.pcbi.1007805.

- David H. Wolpert. The stochastic thermodynamics of computation. *Journal of Physics A: Mathematical and Theoretical*, 52(19):193001, 2019. doi: 10.1088/1751-8121/ab0850.
- David H. Wolpert, Jan Korbelt, Christopher W. Lynn, Farita Tasnim, Joshua A. Grochow, Gülce Kardes, et al. Is stochastic thermodynamics the key to understanding the energy costs of computation? *Proceedings of the National Academy of Sciences*, 121(40):e2321112121, 2024. doi: 10.1073/pnas.2321112121.
- Min Yan, Can Huang, Peter Bienstman, Peter Tino, Wei Lin, and Jie Sun. Emerging opportunities and challenges for the future of reservoir computing. *Nature Communications*, 15:2056, 2024. doi: 10.1038/s41467-024-45187-1.
- H. Peyton Young. The evolution of conventions. *Econometrica*, 61(1):57–84, 1993. doi: 10.2307/2951778.